Climate-related signals in the GV7-C ice core from East Antarctica for 1782–2013 CE: Potential relevance to climate and teleconnections between the tropics and Antarctica

Yalalt Nyamgerel[1], Yeongcheol Han[2], Soon Do Hur[2], Hyemi Kim[3], Songyi Kim[2], Jangil Moon[2], Barbara Stenni[4], Jeonghoon Lee[3]*

[1]Institute of Chemistry and Chemical Technology, Mongolian Academy of Sciences, Ulaanbaatar 13270, Mongolia
[2]Division of Glacier and Earth Sciences, Korea Polar Research Institute, Incheon 21990, Republic of Korea
[3]Department of Science Education, Ewha Womans University, Seoul 120-750, Republic of Korea
[4]Department of Environmental Sciences, Informatics and Statistics, Ca' Foscari University, Venice 30123, Italy

Correspondence to: Jeonghoon Lee (jeonghoon.d.lee@gmail.com)

Abstract. Polar ice cores provide valuable archives of past climate variability, but interpreting these records in coastal East Antarctica remains challenging because multiple meteorological processes can influence the signals preserved in ice cores. Here we investigate climate-related signals in the GV7-C ice core from East Antarctica (1782–2013 CE) using annual records of water isotopes ($\delta^{18}O$ and d-excess) and snow accumulation by comparing them with large-scale climate indices and reanalysis-based climate data. Snow accumulation shows strong interannual variability, suggesting multiple and potentially competing controls, and is weakly linked to sea-surface temperature variability over the Indian Ocean sector (1957–2013 CE). $\delta^{18}O$ exhibits weak but detectable relationships with Pacific-sector variability for 1957–2013 CE, whereas d-excess shows clearer relationships with sea-surface temperature variability in the Indian Ocean sector. Over the longer period (1872–2013 CE), $\delta^{18}O$ correlations generally weaken, implying time-varying controls, while d-excess retains persistent relationships, highlighting its utility for tracking moisture-source conditions. Overall, the GV7-C record suggests potential teleconnections between Antarctic coastal climate and tropical ocean variability.

1 Introduction

Climate variability over Antarctica and the surrounding Southern Ocean is crucial for the global climate system (Mayewski et al., 2009; Fretwell et al., 2013; Rintoul et al., 2018). However, the Antarctic climate system is complex (Masson-Delmotte et al., 2008), with large variations in near-surface air temperature (Nicolas and Bromwich, 2014; Constable et al., 2022) and surface mass balance (Dalaiden et al., 2020a), sparse observational coverage, and high natural variability (Klein et al., 2019; Kim et al., 2020), which is particularly pronounced in coastal regions (Tuohy et al., 2015; Stenni et al., 2017; Goursaud et al., 2019). Ice-core records provide a means to reconstruct past climatic and environmental conditions. Stable water isotopes ($\delta^{18}O$ and δD) in ice cores can reflect relative changes in temperature (Jouzel et al., 1997; Markle and Steig, 2022), sea ice extent (SIE), and atmospheric circulation (Thomas and Abram, 2016). Atmospheric circulation patterns have been reported as important factors influencing isotopic signals in Antarctic ice cores (Bertler et al., 2004; Kino et al., 2021; Leroy-Dos Santos et al., 2023). The relationships between isotopes, temperature, and surface mass balance depend on the relative contributions of large-scale dynamical and thermodynamic processes (Oerter et al., 2000; Medley et al., 2018; Goursaud et al., 2019; Dalaiden et al., 2020b). Moreover, the influence of the Southern Annular Mode (SAM), which describes shifts in the Southern Hemisphere westerlies (Hall and Visbeck, 2002; Fogt et al., 2012), has been identified in $\delta^{18}O$ and surface mass balance records from coastal Antarctic ice cores (Schlosser et al., 2014; Servettaz et al., 2020). The second-order parameter d-excess (d-excess $= \delta D - 8 \times \delta^{18}O$), which is sensitive to relative humidity and sea-surface temperature (SST) at the moisture source (Jouzel et al., 1982; Delmotte et al., 2000; Uemura et al., 2008), has been used to infer source-region conditions (Stenni et al., 2001; Sodemann and Stohl, 2009). Snow accumulation (SA) rates estimated from ice cores can also respond to changes in moisture availability and circulation, and may increase in warmer climates (Frieler et al., 2015; Palerme et al., 2017) and under low sea-ice conditions in coastal regions (Nyamgerel et al., 2020), although the strength and mechanisms of these relationships can be site dependent (Dalaiden et al., 2020a).

In recent decades, SAM variability has exerted a strong influence on Southern Hemisphere climate (Russell and McGregor, 2010), affecting the spatial variability of temperature, precipitation, and sea ice across Antarctica (Nicolas and Bromwich, 2014; Purich et al., 2016; Kim et al., 2020). Antarctic surface mass balance is also linked to the El Niño–Southern Oscillation (ENSO) (Kim et al., 2020). Teleconnections between Antarctic and tropical climate variability have been reported in ice-core records (Yuan, 2004; Schneider and Steig, 2008), but their expression can be complex, non-stationary, and dependent on timescale and the concurrent state of multiple climate modes (e.g., ENSO and SAM), which can limit their detectability in ice-core records (Divine et al., 2009; Turner et al., 2009).

There remains considerable ambiguity regarding the geographical extent and temporal stability of climate signals derived from Antarctic ice cores (Stenni et al., 2017). Differences in spatial and temporal variability indicate the need for additional regionally focused records, particularly in coastal East Antarctica (Vance et al., 2016; Goursaud et al., 2017). The GV7-C ice core site, characterized by relatively high snow accumulation, provides a well-dated and high-resolution record (Caiazzo et al., 2017; Nardin et al., 2021). Here we explore climate-related signals in annual GV7-C records of $\delta^{18}O$, d-excess, and SA for

1782–2013 CE. We compare these records with climate variables at annual and seasonal timescales, recognizing that ice-core isotopic signals integrate source conditions, transport pathways, and rainout processes (Jackson et al., 2023). Particular attention is given to potential remote influences from ENSO and SAM, as suggested by a previous study for 1979–2012 CE (Khan, 2019). Using the GV7-C ice core, this study provides additional insights into potential teleconnections between the tropics and coastal East Antarctica.

2 Materials and methods

2.1 Study area

During the 2013/14 Antarctic summer season, a collaborative Italian/Korean expedition drilled several firn–ice cores at the GV7 drilling site (70°41′ S, 158°52′ E; 1950 m a.s.l.) on the Oates Coast, East Antarctica (Fig. 1). Six shallow firn cores (5–50 m) and intermediate firn–ice cores (78–250 m) were recovered; the 78 m core (GV7-C) is used in this study. The site is approximately 95 km from the nearest coastline of the Southern Ocean, although the distance to open water varies seasonally with sea-ice conditions. Ice velocity at this location is very low (< 0.3 m yr–1), and the 10 m firn temperature is –31.8 °C (Frezzotti et al., 2007). Snow accumulation ranges from 205 to 252 mm w.e. yr–1 (Magand et al., 2004; Frezzotti et al., 2007; Nardin et al., 2021), which is relatively high compared with that at other inland Antarctic sites (e.g., Stenni et al., 2002; Ekaykin et al., 2004) and some coastal sites (Stenni et al., 1999; Nyamgerel et al., 2020; Nyamgerel et al., 2021), and is expected to provide better preservation of seasonal signals and facilitate annual-layer identification (Frezzotti et al., 2007). Moreover, post-depositional effects are expected to be limited due to the low intensity of katabatic winds along the ice divide (Magand et al., 2004; Frezzotti et al., 2007). Back-trajectory and precipitation-source analyses for 2007–2012 (Caiazzo et al., 2017) indicate that the dominant air-mass influence varies seasonally (e.g., enhanced western Pacific influence in autumn–winter and Ross Sea influence in spring), while overall trajectory statistics show frequent pathways from the Indian Ocean sector (32%) and the Antarctic Plateau (29%), with smaller contributions from the Ross Sea (21%) and western Pacific (19%). The western Pacific and Indian Ocean sectors account for ~59% (147 mm) and ~28% (69 mm) of total precipitation (250 mm), respectively (Caiazzo et al., 2017). Snow accumulation at GV7 is estimated to be higher in austral summer and autumn, with a secondary winter maximum associated with pathways from the Antarctic Plateau and the Indian Ocean sector (Caiazzo et al., 2017).

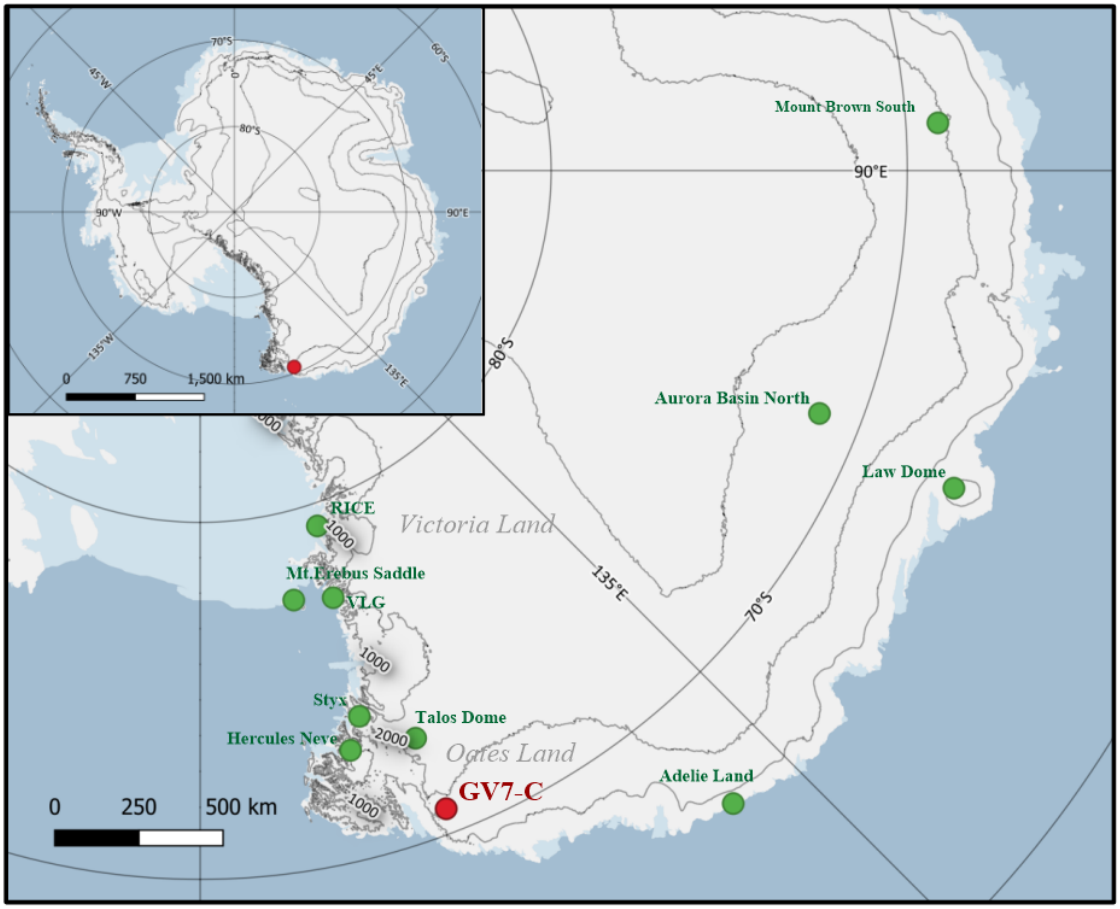


Figure 1. Location of the GV7-C ice core (red) and other ice-core sites (green) in East Antarctica. RAMP2 elevation contours at 1000 m intervals are shown (Liu et al., 2015). The map was generated using QGIS software with Quantarctica3 project data (Matsuoka et al., 2021).

2.2 Ice core data

The 78 m long GV7-C ice core was collected in 107 runs and has an average diameter of ~0.08 m. Density was estimated from the mass and dimensions of core subsections. Core sections were kept frozen and transported to Korea. In the cold room at the Korea Polar Research Institute (KOPRI), the core was cut to an average sample length of 0.04 m (range 0.03–0.07 m) for stable water isotope analysis ($\delta^{18}O$ and δD). A total of 1880 samples were analyzed using cavity ring-down spectrometers (L2130-i and L2140-i, Picarro Inc., USA) at KOPRI. Annual layers were identified from the summer $\delta^{18}O$ maxima, and sample ages were assigned by linear interpolation between consecutive maxima. The GV7-C ice-core record covers 1782–2013 CE. The seasonal $\delta^{18}O$ pattern has been reported previously (Caiazzo et al., 2017; Nardin et al., 2021). Annual-layer counting was further constrained using electrical conductivity measurements with a portable ECM unit (Icefield Instruments Inc., Canada). Conductivity peaks associated with the Pinatubo (1991 CE), Agung (1963 CE), Tarawera (1886 CE), Krakatau (1883 CE), and Tambora (1815 CE) eruptions were used as additional time markers. Annual mean $\delta^{18}O$, δD, and d-excess were calculated as the arithmetic mean of all isotope measurements assigned to each annual layer (i.e., between two successive summer maxima). The annual mean SA rate was estimated by multiplying the annual-layer thickness by the measured density of the corresponding core sections and is reported in millimeters water equivalent per year (mm w.e. yr–1). The number of samples per year ranged from 3 to 21 (average 8); therefore, not all seasons are resolved in every year, and seasonal means are not consistently available. Accordingly, annual means of $\delta^{18}O$, d-excess, and SA are used in the correlation analyses.

2.3 Climate data and analysis

The $\delta^{18}O$ (used in preference to $\delta^{2}H$ because the two are highly correlated; r = 0.99), d-excess, and SA records from the GV7-C ice core were used in the correlation analyses. Two time periods (1957–2013 CE and 1872–2013 CE) were selected for the correlation analyses between the GV7-C records and climate variables, based on data availability (e.g., SAM indices) and the need for an adequate sample size. Annual means of the ice-core records, each derived from multiple intra-annual samples (3–21 data points per year; average 8), were used in the correlation analyses; this averaging reduces the influence of seasonal extreme values. Because the isotopic composition recorded in an annual layer reflects integrated snowfall throughout the year, the GV7-C records represent the combined influence of seasonal processes. We therefore examined the climate data at both annual (January–December) and seasonal (DJF, MAM, JJA, SON) scales to assess potential relationships. Although some seasonal differences were observed, overall patterns and physical interpretations were consistent when annual means were used; therefore, annual values are presented to represent the net integrated climate signal preserved in the ice core.

The correlation analyses were conducted on original and linearly detrended time series (annual values and three-year running averages) of the ice-core and climate data, and the results are described in Sections 3.3.1 and 3.3.2. Correlation analyses on the smoothed time series were conducted to reduce stratigraphic noise; averaging over at least three years has been suggested for obtaining a significant climatic signal at the GV7 site (e.g., Schlosser and Oerter, 2002; Frezzotti et al., 2007; Khan, 2019). Pearson correlation coefficients were calculated, and their significance was assessed using a two-tailed Student's t-test, with the corresponding p-values reported. Although the ice-core and climate data were annually averaged and linear trends were removed, the effects of autocorrelation on the correlation analyses were also tested using the effective number of degrees of freedom (Neff; Bretherton et al., 1999) at $p < 0.05$. The results indicated negligible autocorrelation effects on the reported correlations (Tables 4 and 6), and thus the correlations can be considered statistically robust.

For the 1957–2013 CE period, the following climate indices, expressed as annual means (January–December), were compared with the annual means of the GV7-C ice-core records: the station-based SAM index (Marshall, 2003; Marshall and National Center for Atmospheric Research Staff, 2018); the Southern Oscillation Index (SOI) obtained from the National Centers for Environmental Information (NCEI) (available at https://www.ncei.noaa.gov/access/monitoring/enso/soi); the Niño3.4 index (5°S–5°N, 170°W–120°W) (Rayner et al., 2003; available at https://psl.noaa.gov/gcoswgsp/Timeseries/Nino34); the Indian Ocean Dipole (IOD) index, i.e., the Dipole Mode Index, representing the SST gradient between the western (50°E–70°E, 10°S–10°N) and southeastern (90°E–110°E, 10°S–0°) equatorial Indian Ocean (IO) (available at https://psl.noaa.gov/gcos_wgsp/Timeseries/DMI); the SST anomaly in the southeastern IO (SST-SEIO) (90°E–110°E, 10°S–0°) (available at https://psl.noaa.gov/gcos_wgsp/Timeseries/Data/dmieast.had.long.data); and reconstructed sea ice extent over the Ross–Amundsen Sea sector (SIE-RA; 162°E–250°E) and the East Antarctic sector (SIE-EA; 71°E–162°E) (Fogt et al., 2023). Moreover, for the 1957–2013 CE period, spatial correlation analyses (at the 95% confidence level) were conducted between the annual GV7-C records and gridded ERA5 reanalysis data produced by the European Centre for Medium-Range

Weather Forecasts (ECMWF) (air temperature, SST, sea ice concentration [SIC], 10-m wind speed, zonal [u] and meridional [v] wind components, and total precipitable water) using Climate Reanalyzer, developed by the University of Maine, USA (https://climatereanalyzer.org/). ERA5 shows better performance than its predecessor, ERA-Interim, owing to its higher spatial and temporal resolution, improved model physics and core dynamics, and data assimilation (Hersbach et al., 2020), and it also performs well overall compared with other reanalysis products (Caton Harrison et al., 2022; Marshall et al., 2022). ERA5 effectively represents temperature variability over Antarctica, particularly for annual and seasonal mean temperatures and at higher-elevation sites (>1000 m a.s.l.), although some biases and regional differences have been reported (Tetzner et al., 2019; Zhu et al., 2021). We acknowledge that ERA5 has been used mainly for the satellite era (from 1979 onward), when observational coverage was better than during the pre-satellite period, particularly over Antarctica and the Southern Ocean (Hersbach et al., 2020), and that it has been widely applied in Antarctic ice-core studies (Leroy-Dos Santos et al., 2023; Thomas et al., 2024; Kim et al., 2025). However, studies using ERA5 for the pre-satellite period (1950–1979) have also reported good performance (Marshall et al., 2022; Xie et al., 2023). In this study, we therefore used ERA5 reanalysis data for the period 1957–2013 CE in the spatial correlation analyses. Because ice-core signals reflect a broad range of thermodynamic and dynamic influences, these spatial correlation analyses were conducted for physically plausible scenarios to help identify potential moisture-supply regions over a longer time period (1957–2013 CE) than in previous studies (Caiazzo et al., 2017; Khan, 2019). As mentioned above, the 1957–2013 CE period was selected because of data availability (e.g., SAM indices) and because it provides longer temporal coverage than previous studies. Spatially coherent and physically interpretable patterns are selectively presented and used as supporting evidence in the interpretation of climate-related signals from the GV7-C ice core. Principal component analysis (PCA), a linear dimensionality reduction technique, was employed to investigate potential similarities in variability between the annual means of the ice-core records and the seasonal and annual means of the climate datasets (IOD, SST-SEIO, SAM, SOI, Niño3.4, SIE-EA, SIE-RA) for 1957–2013 CE. Only the PCA results based on annual mean values are presented in this study.

For the 1872–2013 CE period, the GV7-C ice-core data were compared with the following climate indices, expressed as annual means (January–December): the IOD index, SST-SEIO, and Niño3.4 index described above; the reconstructed SST anomaly over the Southern Hemisphere (SST-SH) (Huang et al., 2017; available at https://www.ncei.noaa.gov/access/monitoring/climate-at-a-glance/global/time-series); and the reconstructed SAM index from the NOAA-CIRES-DOE Twentieth Century Reanalysis (20CR) (available at https://psl.noaa.gov/data/20thC_Rean/timeseries/monthly/SAM). SAM and ENSO are considered key modes potentially affecting Antarctic climate variability (Turner et al., 2009; Cohen et al., 2013; Pohl et al., 2021; Wille et al., 2021), and the SOI and Niño3.4 indices describe Pacific variability that can influence the climate of the Southern Ocean and Antarctica (Meyerson et al., 2002; Bertler et al., 2004). Moreover, SST anomalies over the Indian Ocean (as represented by the IOD index and SST-SEIO) affect air temperature (Zhang and Duan, 2023), sea ice extent (Kim et al., 2023; Zhang et al., 2024), and precipitation (Lee and Jin, 2024) in Antarctica.

3 Results and discussion

3.1 Characterization of the GV7-C ice core record

The descriptive statistics for the annual mean δ18O, δD, d-excess, and SA in the GV7-C ice core are presented in Table 1. The results are also presented for five sub-periods of approximately 50 years each (Table 1). Linear regressions of δD and d-excess against δ18O are reported for the entire dataset and for the five sub-periods, as well as for annual means, annual maxima, and annual minima (Table 2). For the whole 1782–2013 CE period, the annual mean δ18O in the GV7-C ice core (n = 233) ranged from –32.92‰ to –24.60‰, while δD ranged from –259.42‰ to –191.43‰. The annual variations in δ18O, d-excess, and SA are presented in Fig. 2 and reveal large interannual and decadal-scale variability. Periods of at least five consecutive years with δ18O lower (i.e., colder) than the average (–29.64‰) were observed seven times (1838–1842 CE, 1858–1862 CE, 1880–1885 CE, 1904–1908 CE, 1918–1922 CE, 1960–1965 CE, and 1995–2002 CE). In addition, δ18O was below average throughout 1977–1991 CE, except in 1979, 1982, 1985, and 1990 CE. Conversely, periods of at least six consecutive years with above-average δ18O occurred in 1787–1801 CE, 1807–1813 CE, 1937–1942 CE, and 1948–1958 CE (except 1953 CE) (Fig. 2). The linear relationship between δ18O and δD ($\delta D = 8.46 \times \delta 18O + 17.97$, $R2 = 0.99$, $n = 1880$, $p < 0.001$) has a slope slightly larger than that of the global meteoric water line (8; Craig, 1961) and that of the Antarctic-wide relationship (7.75; Masson-Delmotte et al., 2008). The slopes derived for the five sub-periods ranged from 8.35 (1982–2013 CE) to 8.67 (1882–1931 CE) (Table 2).

The annual d-excess ranged from 1.70‰ to 7.61‰ (n = 233) (Table 1). Periods of at least five consecutive years with d-excess above the mean were observed in 1786–1790 CE, 1855–1861 CE, 1884–1888 CE, 1903–1911 CE, 1932–1940 CE, 1951–1956 CE, 1962–1966 CE, and 1974–1978 CE, while periods of at least five consecutive years with d-excess below the mean occurred in 1798–1802 CE, 1840–1848 CE, 1922–1926 CE, 1985–1990 CE, and 2006–2011 CE (Fig. 2). A positive correlation was observed between δ18O and d-excess ($r = 0.45$, $p < 0.001$, $n = 1880$) (Table 2), suggesting that both are linked to climatic conditions in the moisture-source region. The slopes of the d-excess–δ18O relationship varied slightly among the sub-periods, but the correlation remained positive throughout (Table 2). This suggests a relatively consistent (i.e., oceanic) moisture source for the GV7-C site. It can therefore be assumed that the variations in δ18O and d-excess in the GV7-C ice core are indicative of ocean surface conditions (e.g., humidity, SST, and wind speed) (Uemura et al., 2008).

The annual mean SA ranged from 79 to 460 mm w.e. yr–1 in the GV7-C ice core, with a long-term mean of 223 ± 59 mm w.e. yr–1 (Table 1). Strong interannual variation was observed, with no long-term trend over the 1782–2013 CE period. Periods of at least four consecutive years with SA above the mean (223 mm w.e. yr–1) were observed in 1784–1787 CE, 1896–1899 CE, and 1999–2002 CE, while SA was below the mean during 1878–1883 CE and 1945–1952 CE (Fig. 2). The mean SA in the GV7-C ice core is comparable to values previously reported for nearby cores (205–252 mm w.e. yr–1) (Frezzotti et al., 2007; Caiazzo et al., 2017; Khan, 2019; Nardin et al., 2021) and for other coastal regions of East Antarctica (Table 3).

Table 1. Descriptive statistics for the annual means of the GV7-C ice core data.

Years (CE)	Long-term (1782–2013)	1782–1831	1832–1881	1882–1931	1932–1981	1982–2013
			$\delta^{18}O$ (‰)			
Mean	–29.64	–29.24	–29.78	–29.88	–29.49	–29.90
Standard Deviation	1.26	1.02	1.41	1.09	1.28	1.45
Minimum	–32.92	–32.72	–32.92	–32.34	–32.74	–31.96
Maximum	–24.60	–26.86	–24.60	–27.39	–27.14	–24.84
			δD (‰)			
Mean	–232.69	–229.59	–233.76	–234.69	–231.76	–234.17
Standard Deviation	10.37	8.42	11.50	9.31	10.50	11.91
Minimum	–259.42	–259.42	–258.36	–255.61	–258.98	–250.66
Maximum	–191.43	–210.21	–191.43	–213.50	–212.01	–192.08
			d-excess (‰)			
Mean	4.43	4.33	4.44	4.36	4.20	5.02
Standard Deviation	1.07	0.88	1.08	1.25	1.03	0.97
Minimum	1.70	2.25	2.21	1.70	2.42	2.98
Maximum	7.61	6.34	6.99	7.61	7.07	6.64
			Snow accumulation (mm w.e. yr^{-1})			
Mean	223.01	225.06	217.80	227.03	219.76	226.70
Standard Deviation	58.77	68.97	48.93	54.91	59.15	63.50
Minimum	79.02	101.79	143.06	81.37	107.58	79.02
Maximum	459.88	459.88	307.94	319.04	340.61	343.92

Table 2. Linear regression analysis for $\delta^{18}O$ with δD and *d*-excess from the GV7-C ice core.

	Slope	Intercept	R^2	*p*-value	n
		$\delta^{18}O$ vs δD			
1782–2013 CE (all data)	8.46	17.97	0.99	<0.0001	1880
1782–1831 CE	8.54	20.12	0.99	<0.0001	344
1832–1881 CE	8.44	17.60	0.99	<0.0001	355
1882–1931 CE	8.67	24.36	0.99	<0.0001	399
1932–1981 CE	8.51	19.41	0.99	<0.0001	429
1982–2013 CE	8.35	15.51	0.99	<0.0001	353
Annual mean	8.17	9.64	0.99	<0.0001	233
Annual maximum	8.27	13.57	0.98	<0.0001	233
Annual minimum	8.19	9.07	0.99	<0.0001	233
		$\delta^{18}O$ vs *d*-excess			
1782–2013 CE (all data)	0.46	18.07	0.21	<0.0001	1880
1782–1831 CE	0.54	20.04	0.24	<0.0001	344
1832–1881 CE	0.45	17.83	0.18	<0.0001	355
1882–1931 CE	0.67	24.33	0.34	<0.0001	399
1932–1981 CE	0.52	19.45	0.24	<0.0001	429
1982–2013 CE	0.36	15.62	0.18	<0.0001	353
Annual mean	0.18	9.68	0.04	<0.0001	233
Annual maximum	0.28	14.45	0.10	<0.0001	233
Annual minimum	0.26	10.68	0.09	<0.0001	233

Table 3. Comparison of the mean snow accumulation rate from the GV7-C ice core with previous ice core records in this location and other East Antarctic ice cores.

Location	Approximate distance to GV7-C, km	Snow accumulation, mm w.e yr^{-1}	Period (CE)	Reference
GV7-C	–	223 ± 59	1782–2013	This study
GV7 site	–	252 ± 104	2001–2004	Frezzotti et al., 2007
GV7 site	–	242 ± 71	2007–2013	Caiazzo et al., 2017
GV7 site	–	250 ± 85	2008–2013	Caiazzo et al., 2017
GV7 site	–	238.7 ± 13	1979–2012	Khan, 2019
GV7 site	–	241 ± 13	1965–2001	Magand et al., 2004
GV7 site	–	242 ± 57	1965–2000	Nardin et al., 2021
GV7 site	–	233 ± 64	1854–2004	Nardin et al., 2021
GV7 site	–	205 ± 63	1179–2009	Nardin et al., 2021
RICE	972	210	1965–2017	Winstrup et al., 2019
Mt. Erebus Saddle	811	230	1950–2006	Rhodes et al., 2012
Styx-B	394	146 ± 60	1990–2014	Nyamgerel et al., 2020
Hercules Névé	348	119	1770–1992	Stenni et al., 1999
VLG (Victoria Lower Glacier)	700	30	1808–2000	Bertler et al., 2011
Talos Dome	239	80	1232–1995	Stenni et al., 2002
Adelie Land	884	218 ± 69	1946–2006	Goursaud et al., 2017
Law Dome	1855	688	22 BCE to 2012	Roberts et al., 2015
Aurora Basin North	1713	119	1979–2013	Servettaz et al., 2020
Mount Brown South	2648	263 ± 46	1979–2016	Jackson et al., 2023

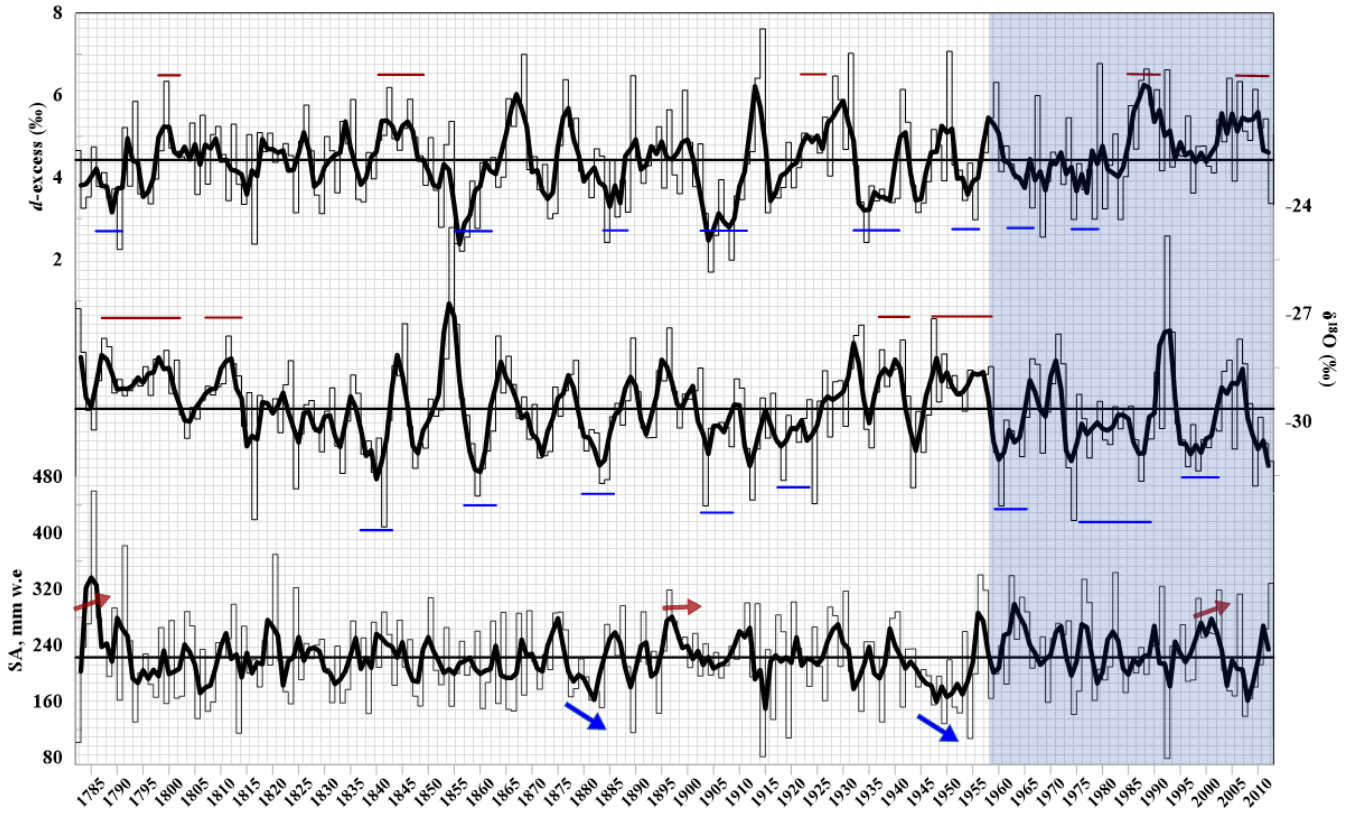


Figure 2. Temporal variations in SA (bottom panel), δ18O (middle panel), and d-excess (top panel). Horizontal black lines indicate the overall means, and thick black lines represent 3-year running averages. Blue and red arrows indicate periods of at least four consecutive years with values below or above the mean, respectively. Blue shading marks the 1957–2013 CE period discussed in Section 3.2.

3.2 Spatial correlation analysis with ERA5 reanalysis

Spatial correlation analyses (95% confidence level) were conducted between annual GV7-C records ($\delta^{18}O$, d-excess, and SA) and annual/seasonal ERA5 reanalysis fields for 1957–2013 CE to explore potential spatial patterns consistent with moisture supply and transport pathways. Because ice-core signals reflect a broad range of influencing factors, the analyses were conducted at both annual and seasonal timescales and at different pressure levels, considering several physically plausible variables, including air temperature, SST, SIC, wind speed, zonal and meridional wind components, and total precipitable water. These analyses were primarily intended to highlight potential relationships and provide supporting evidence for moisture-source regions based on the spatial coherence of different climate variables over the 1957–2013 CE period. Significant ($|r| > 0.3$ at the 95% confidence level) and physically interpretable patterns were selected and are presented in the Supplement (Figs. S1–S3) as supporting evidence for the interpretation of potential climate-related signals in the GV7-C ice core. For interpretation, the Pacific Ocean (PO) sector is defined here as the western Pacific (90–160°E), the Ross Sea (160°E–130°W), and the Amundsen–Bellingshausen Seas (130–60°W), while the IO sector is defined as 20–90°E.

Annual mean $\delta^{18}O$ shows positive correlations with 2 m air temperature and SST primarily over the PO sector (Fig. S1a, b). Positive relationships with air temperature (2 m and 850 hPa) and total precipitable water are most evident during DJF over parts of the PO and IO sectors (Fig. S1d–f). Negative correlations are observed with SIC over the Ross Sea region (Fig. S1c). Wind-speed correlations (10 m; DJF and MAM) are generally negative (Fig. S1g, j), and zonal wind (u-wind) correlations highlight the belt of strong westerlies (Fig. S1h, k). The meridional wind (v-wind) correlations suggest a northward flow signature over the western PO sector and a southward flow signature over the IO sector during DJF (Fig. S1i), whereas these patterns weaken in MAM (Fig. S1l). Overall, $\delta^{18}O$ exhibits its clearest spatial coherence during DJF and MAM, consistent with the seasonality of transport and snowfall in this coastal sector (Delmotte et al., 2000; Caiazzo et al., 2017). These patterns provide qualitative support for a stronger PO-sector influence on $\delta^{18}O$ at GV7-C during DJF–MAM, although the overall relationships remain modest.

Annual mean d-excess exhibits positive correlations with air temperature (2 m and 850 hPa) over both the western PO and IO sectors (Fig. S2a–c). Temperature correlations in the IO sector are particularly evident in SON (Fig. S2c), whereas the d-excess response to temperature appears weaker in DJF (not shown). Correlations with SST (SON), SIC (JJA), and total precipitable water (annual) further support a contribution of air masses from the IO sector and the western PO sector to the GV7 region (Fig. S2d–f). In contrast to $\delta^{18}O$, correlations with wind speed and wind direction are relatively weak, except for a positive correlation with 10 m wind speed in some regions (Fig. S2g). The v-wind pattern indicates a southward flow signature over the IO sector and a northward flow signature over the western PO sector (Fig. S2i). Taken together, these spatial patterns suggest that thermodynamic source-region variability (e.g., SST and air-temperature conditions) may play a larger role in d-excess at GV7-C than do purely dynamical indicators, and they are consistent with a potentially important contribution from the IO sector, particularly during SON.

No clear and temporally consistent relationships are observed between SA and the investigated climate variables; only weak and spatially limited patterns are identified (Fig. S3). For example, SA shows weak negative correlations with 2 m temperature over parts of the Amundsen Sea coast and weak positive correlations with total precipitable water off the Ross Sea coast (Fig. S3a, b). SA also shows weak negative correlations with SIC over the Ross Sea region (Fig. S3c). Wind-speed correlations (10 m and 850 hPa) are weakly positive over parts of the PO sector (Fig. S3d, g), and the associated u- and v-wind patterns suggest modest transport signals (Fig. S3e, f, h, i). Overall, these results indicate that SA at GV7-C is likely influenced by multiple factors, including synoptic variability and transport efficiency, which may mask simple relationships with large-scale indices at annual resolution.

In sum, the results of the spatial correlation analyses (Figs. S1–S3) suggest that the GV7-C ice core can be used to represent regional climate conditions over the PO and IO sectors. The correlations observed with $\delta^{18}O$ during DJF and MAM led us to consider the potential influence of SAM, at least over the 1957–2013 CE period. It is conceivable that a positive phase of SAM during DJF and MAM could strengthen the climate signals recorded at GV7-C, allowing SAM-related signals to be detectable in $\delta^{18}O$ and SA during the 1957–2013 CE period. The dynamical influence of SAM can thus be important for $\delta^{18}O$ and SA, while d-excess is likely to represent thermodynamic changes over the IO and western PO sectors, particularly during SON. These correlations for d-excess may be remotely linked to temperature variability over the tropical IO and PO (Masson-Delmotte et al., 2003).

3.3 Correlation analysis for 1957–2013 CE and 1872–2013 CE periods

3.3.1 Climate signals for the 1957–2013 CE period

The SAM, Niño3.4, SOI, IOD, SST-SEIO, SIE-EA, and SIE-RA data were compared with the $\delta^{18}O$, d-excess, and SA records of the GV7-C ice core. The standardized values of these variables for 1957–2013 CE are presented in Fig. 3. $\delta^{18}O$ exhibited three periods of higher values (1964–1971 CE, 1989–1993 CE, and 2001–2007 CE) (Fig. 3), while d-excess remained generally flat before 1983 CE and showed two periods of higher values (1985–1992 CE and 2002–2011 CE). SA showed strong interannual variability. Pearson's correlation coefficients (r) between the GV7-C ice-core records and the climate variables are shown in Table 4. Correlations were calculated for annual values and three-year running averages of the detrended time series. Correlations for the original (non-detrended) time series are also shown for comparison, and the results were comparable (Table 4). For the annual mean time series, no significant correlations were found, except for a weak correlation between SA and the IOD ($r = 0.37$, $p < 0.05$, $n = 57$). In the three-year running-averaged time series, SA retained weak correlations with the IOD ($r = 0.39$, $p < 0.01$, $n = 55$) and SST-SEIO ($r = –0.30$, $p < 0.05$, $n = 55$). $\delta^{18}O$ exhibited correlations with SAM ($r = –0.41$, $p < 0.005$, $n = 55$), SOI ($r = –0.49$, $p < 0.001$, $n = 55$), Niño3.4 ($r = 0.46$, $p < 0.001$, $n = 55$), and SIE-RA ($r = –0.47$, $p < 0.001$, $n = 55$) in the three-year running-averaged time series. For d-excess, there was a moderate correlation with SST-SEIO ($r = 0.64$, $p < 0.001$, $n = 55$) and weak correlations with the IOD ($r = –0.45$, $p < 0.001$, $n = 55$) and SIE-EA ($r = –0.35$, $p < 0.01$, $n = 55$). Overall, the correlation analysis suggests that variations in $\delta^{18}O$ during 1957–2013 CE reflect climatic signals from both the tropical and southern sectors of the PO, indicating possible contributions from air masses originating in these regions. In contrast, variations in d-excess appear to reflect SST variability in the southeastern IO, suggesting a possible influence of air masses originating in that region. Moreover, climatic conditions over the IO sector appear to be reflected in the SA record of the ice core. Considering the seasonality of Niño3.4 and the IOD, their relationships with the GV7-C ice-core records were also examined at the seasonal scale (not shown). For the three-year running-averaged time series, Niño3.4 showed positive correlations only with $\delta^{18}O$, in all seasons ($r = 0.33–0.43$, $p < 0.05$, $n = 55$), with the strongest correlation occurring in MAM. In contrast, the IOD showed negative correlations with d-excess during JJA ($r = −0.53$, $p < 0.001$, $n = 55$) and MAM ($r = −0.51$, $p < 0.001$, $n = 55$) for the three-year running-averaged time series. Moreover, the IOD showed weak positive correlations with SA in MAM ($r = 0.31$, $p < 0.05$, $n = 57$) for the annual time series, and in JJA ($r = 0.36$, $p < 0.05$, $n = 55$) and SON ($r = 0.36$, $p < 0.05$, $n = 55$) for the three-year running-averaged time series. These seasonal relationships are generally consistent with the results of the spatial correlation analyses (Section 3.2). Although this study is primarily based on annual climate indices, further investigation using seasonally resolved climate indices and event-based analyses would be valuable for better understanding the seasonal mechanisms linking climate indices to the GV7-C ice-core records.

PCA was conducted for 1957–2013 CE, with the loading matrix (correlation coefficients at $p < 0.05$) presented in Table 5. Principal component (PC) 1 grouped $\delta^{18}O$, SAM, SOI, Niño3.4, SIE-EA, and SIE-RA. This reflects the importance of both thermodynamic and dynamical effects: $\delta^{18}O$ decreases (increases) with increased (decreased) SIE, stronger (weaker) westerlies

associated with positive (negative) SAM conditions, and higher (lower) SOI values together with lower (higher) SST anomalies in the Niño3.4 region, corresponding to La Niña (El Niño)-like conditions. In PC 2, d-excess and SA were grouped with the IOD, SAM, and SIE, with a particularly strong loading of SST-SEIO. This likely represents increasing (decreasing) d-excess with enhanced (reduced) evaporation under warm (cold) SSTs, particularly over the southeastern IO. In addition, there may be a weak association with enhanced (weakened) air-mass transport by strong (weak) westerlies under positive (negative) SAM conditions, a consequent wind-induced increase (decrease) in SIE over East Antarctica, and relatively warmer (cooler) temperatures over the eastern IO (i.e., a decreasing (increasing) IOD). The negative correlation between SA and SST-SEIO in PC 2 is difficult to explain. In contrast to the expected positive influence of warmer source-region SSTs on moisture availability and precipitation, the observed negative relationship may reflect the combined effects of atmospheric circulation, moisture transport pathways, and precipitation efficiency, rather than a direct thermodynamic response to SST alone. PC 3 included only SA among the ice-core records, with stronger loadings of the IOD, SAM, SOI, Niño3.4, and SIE-EA. This may represent thermodynamic effects on SA, with increased (decreased) evaporation under warm (cold) SSTs over the western equatorial IO (i.e., the IOD) and the central tropical PO (i.e., the SOI and Niño3.4), enhanced moisture transport by strong westerlies (i.e., SAM), and wind-induced changes in SIE over East Antarctica. PC 4 was characterized by increasing (decreasing) $\delta^{18}O$ and d-excess with decreasing (increasing) SST-SEIO, which may be explained by the intrusion of different air masses carrying distinct d-excess and $\delta^{18}O$ signals. Overall, the PCA separated the variables into groups representing climatic signals from the PO sector (PC 1) and the southeastern IO sector (PC 2). Interestingly, the relatively strong detectability of the thermodynamic effect on d-excess associated with the IO sector likely indicates that temperature signals from this region are detectable in the GV7-C record.

Table 4. Pearson's correlation coefficients (r) between the GV7-C ice core records and the climate variables, including Indian Ocean Dipole (IOD), sea surface temperature anomaly over the southeastern Indian Ocean (SST-SEIO), Southern Annular Mode (SAM), Southern Oscillation Index (SOI), Niño3.4, sea ice extent over East Antarctica (SIE-EA) and the Ross-Amundsen Sector (SIE-RA) for the period 1957–2013 CE. Correlations are calculated for annual data and three-year running averages in the detrended and original time series (shown in parentheses). Larger values ($r > 0.3$ at $p < 0.05$) are marked in bold.

	IOD	SST-SEIO	SAM	SOI	Niño3.4	SIE-EA	SIE-RA
				Annual average			
SA	**0.37** (0.28)	–0.22 (–0.26)	0.12 (0.04)	–0.00 (–0.01)	0.04 (0.04)	0.01 (–0.02)	0.09 (0.00)
$\delta^{18}O$	–0.01 (–0.03)	–0.06 (–0.07)	–0.18 (–0.18)	–0.26 (-0.26)	0.22 (0.22)	–0.06 (–0.07)	–0.23 (–0.22)
d-excess	–0.19 (–0.07)	0.25 **(0.33)**	–0.03 (0.09)	0.02 (0.03)	0.04 (0.05)	–0.05 (0.02)	0.11 (0.22)
				Three-year running average			
SA	**0.39** (0.18)	**–0.30 (–0.36)**	0.11 (–0.06)	0.09 (0.09)	–0.11 (–0.14)	0.11 (0.04)	–0.18 (–0.02)
$\delta^{18}O$	–0.06 (–0.02)	0.02 (0.04)	**–0.41** (–0.27)	**–0.49 (–0.49)**	**0.46 (0.46)**	–0.14 (–0.11)	**–0.47 (–0.32)**
d-excess	**–0.45** (–0.06)	**0.64 (0.72)**	–0.15 (–0.21)	–0.11 (–0.09)	0.24 (0.27)	**–0.35** (–0.16)	0.01 (0.31)

Table 5. Loadings of the variables, including snow accumulation (SA), $\delta^{18}O$, *d*-excess, Indian Ocean Dipole (IOD), sea surface temperature anomaly over the southeastern Indian Ocean (SST-SEIO), Southern Annular Mode (SAM), Southern Oscillation Index (SOI), Niño3.4, sea ice extent over East Antarctica (SIE-EA) and the Ross-Amundsen Sector (SIE-RA) for the first four principal components (PCs) of the PCA analysis conducted with the data for 1957–2013 CE. Larger values of correlation coefficients ($r > 0.3$, at $p < 0.05$) are marked in underlined bold.

Variables	PC1	PC2	PC3	PC4
SA	0.04	**–0.48**	**0.43**	–0.04
$\delta^{18}O$	**–0.39**	0.20	–0.04	**0.77**
d-excess	0.05	**0.63**	–0.07	**0.49**
IOD	0.12	**–0.30**	**0.77**	0.27
SST-SEIO	–0.07	**0.82**	–0.08	**–0.40**
SAM	**0.52**	**0.30**	**0.56**	–0.08
SOI	**0.82**	–0.23	**–0.43**	0.13
Niño3.4	**–0.80**	0.27	**0.47**	–0.13
SIE-EA	**0.52**	**0.31**	**0.38**	0.00
SIE-RA	**0.84**	0.29	0.13	0.05
Variance explained (%)	*27*	*18*	*17*	*11*
Cumulative percent (%)	*27*	*45*	*62*	*73*

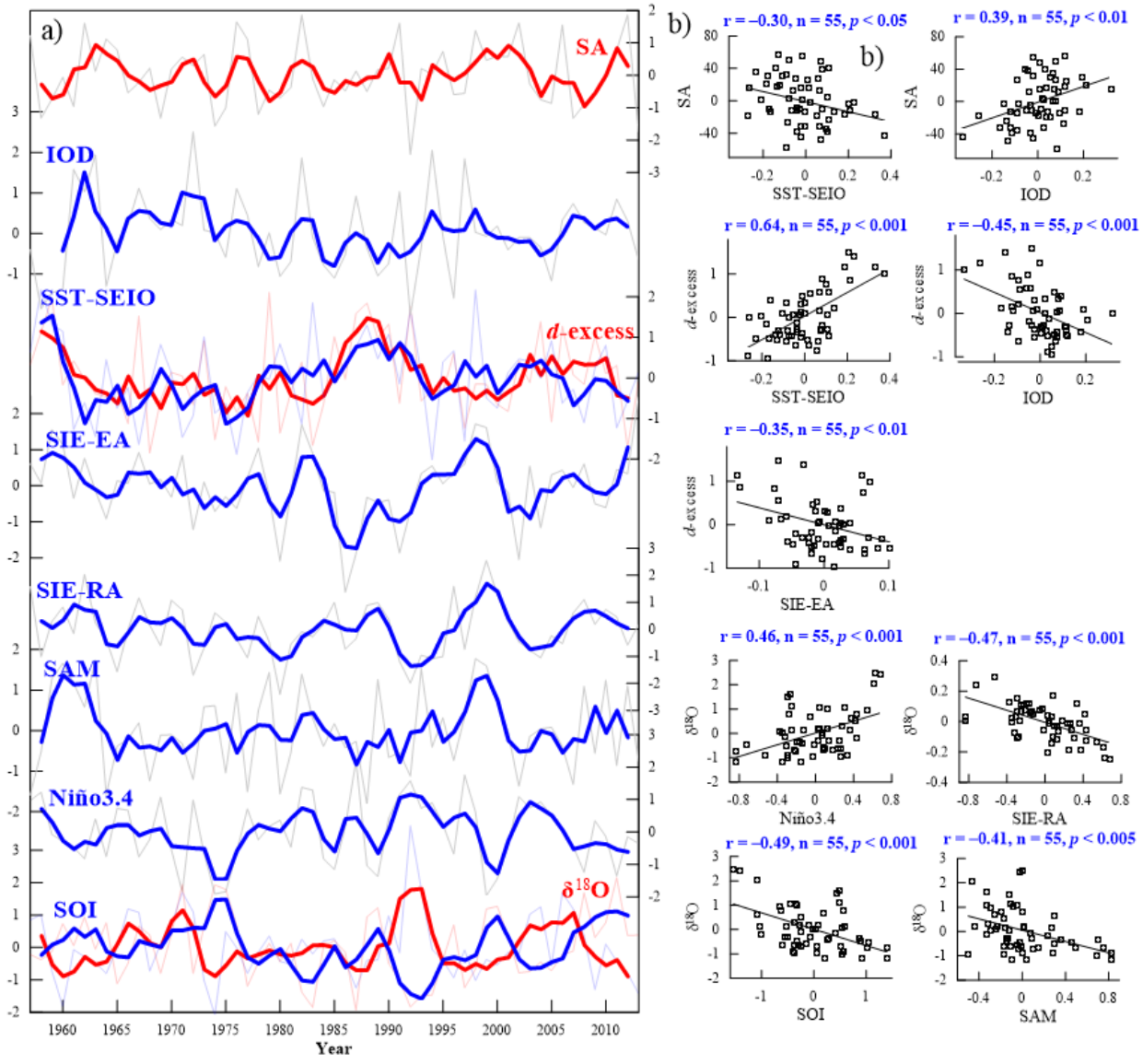


Figure 3. (a) Standardized profiles (grey lines) of the detrended time series of snow accumulation (SA), $\delta^{18}O$, and d-excess compared with those of the climate variables, including the Indian Ocean Dipole (IOD) index, the sea surface temperature anomaly over the southeastern Indian Ocean (SST-SEIO), the Southern Annular Mode (SAM) index, the Southern Oscillation Index (SOI), Niño3.4, and sea ice extent over East Antarctica (SIE-EA) and the Ross–Amundsen Sea sector (SIE-RA) for 1957–2013 CE. Thick lines (blue and red) indicate 3-year running averages. (b) Linear regression lines for the 3-year running-averaged time series, shown with significant correlation coefficients ($p < 0.05$).

3.3.2 Climate signals for the long-term records (1872–2013 CE)

The GV7-C ice-core data were also compared with long-term records (1872–2013 CE) of SAM, Niño3.4, the IOD, SST-SEIO, and SST-SH (Fig. 4 and Table 6). Pearson's correlation coefficients (r) between the GV7-C ice-core records and the climate variables are shown in Table 6. Correlations were calculated for annual values and three-year running averages of the detrended time series. Correlations for the original (non-detrended) time series are also shown for comparison, and the results were comparable (Table 6). For $\delta^{18}O$ and SA, no significant correlations with the climate variables were found for this period. This absence of correlation suggests that the signals are attenuated by various influencing factors over the longer period. The correlations of $\delta^{18}O$ with Niño3.4 ($r = 0.46$) and SOI ($r = -0.49$) for 1957–2013 CE (Table 4) suggest an influence of SST changes in the PO sector; however, these correlations weakened over the longer period (1872–2013 CE). Nevertheless, some relationships can still be seen for $\delta^{18}O$ and SA over shorter intervals. The decrease in SA during the 1876–1885 CE and 1940–1955 CE periods was consistent with the increasing trend in the SAM index. The recent trend (1985–2013 CE) in $\delta^{18}O$ was also in line with those of Niño3.4 and the SAM index (Fig. 4). In contrast, d-excess was correlated with SST-SEIO ($r = 0.32$, $p < 0.001$, $n = 140$) in the three-year running-averaged time series (Table 6 and Fig. 4). The spatial correlation of d-excess with the reconstructed SST dataset is also shown for two periods, 1957–2013 CE and 1854–2013 CE (Fig. 5). Weak positive correlations were observed over the remote IO sector during 1957–2013 CE (Fig. 5a), whereas for 1854–2013 CE, positive correlations were observed over a larger area of the southern IO (Fig. 5b). Although the correlations are weak and do not show clear anomaly patterns associated with SST changes over the PO and IO, the positive correlations observed over the southern IO sector provide some qualitative support for the possibility that the d-excess signal in the GV7-C ice core partly reflects thermodynamic variability (i.e., SST changes) over the IO sector of the Southern Ocean, at least over the 1872–2013 CE period.

Table 6. Pearson's correlation coefficients (r) between the GV7-C ice core records and the climate variables, including Indian Ocean Dipole (IOD), sea surface temperature anomaly over the southeastern Indian Ocean (SST-SEIO) and southern hemisphere (SST-SH), Southern Annular Mode (SAM), and Niño3.4 for the period 1872–2013 CE. Correlations are calculated for annual data and three-year running averages in the detrended and original time series (shown in parentheses). Larger values ($r > 0.3$ at $p < 0.05$) are marked in underlined bold.

	IOD	SST-SEIO	SST-SH	SAM	Niño3.4
			Annual average		
SA	0.10 (0.10)	–0.15 (–0.11)	–0.03 (–0.01)	0.03 (0.03)	0.02 (0.02)
$\delta^{18}O$	–0.04 (–0.04)	–0.01 (–0.02)	–0.10 (–0.08)	–0.16 (–0.14)	0.14 (0.13)
d-excess	–0.02 (0.08)	0.02 (0.28)	–0.20 (0.28)	0.06 (0.18)	0.12 (0.13)
			Three-year running average		
SA	–0.04 (0.01)	–0.02 (0.02)	–0.04 (0.02)	0.00 (0.04)	0.02 (0.03)
$\delta^{18}O$	–0.12 (–0.11)	0.00 (–0.02)	–0.13 (–0.11)	–0.23 (–0.16)	0.19 (0.18)
d-excess	0.03 (0.23)	**0.32 (0.43)**	0.26 **(0.39)**	–0.02 (0.24)	0.24 (0.26)

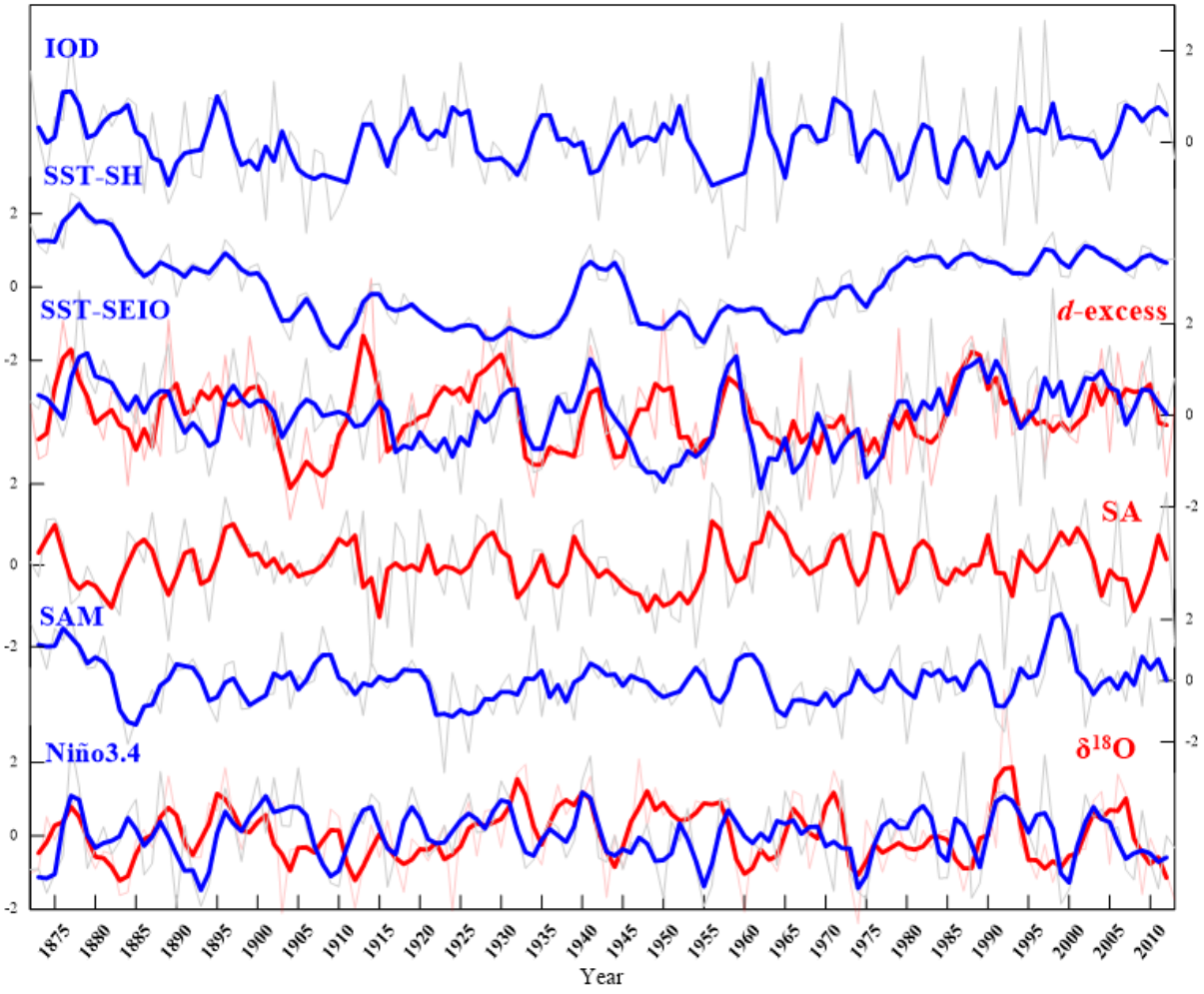


Figure 4. Standardized profiles (thin lines) of the detrended time series of SA, $\delta^{18}O$, and d-excess compared with those of the Indian Ocean Dipole (IOD) index, sea surface temperature anomalies over the southeastern Indian Ocean (SST-SEIO) and over the Southern Hemisphere (SST-SH), the Southern Annular Mode (SAM) index, and Niño3.4 for 1872–2013 CE. Thick lines (blue and red) indicate 3-year running averages.

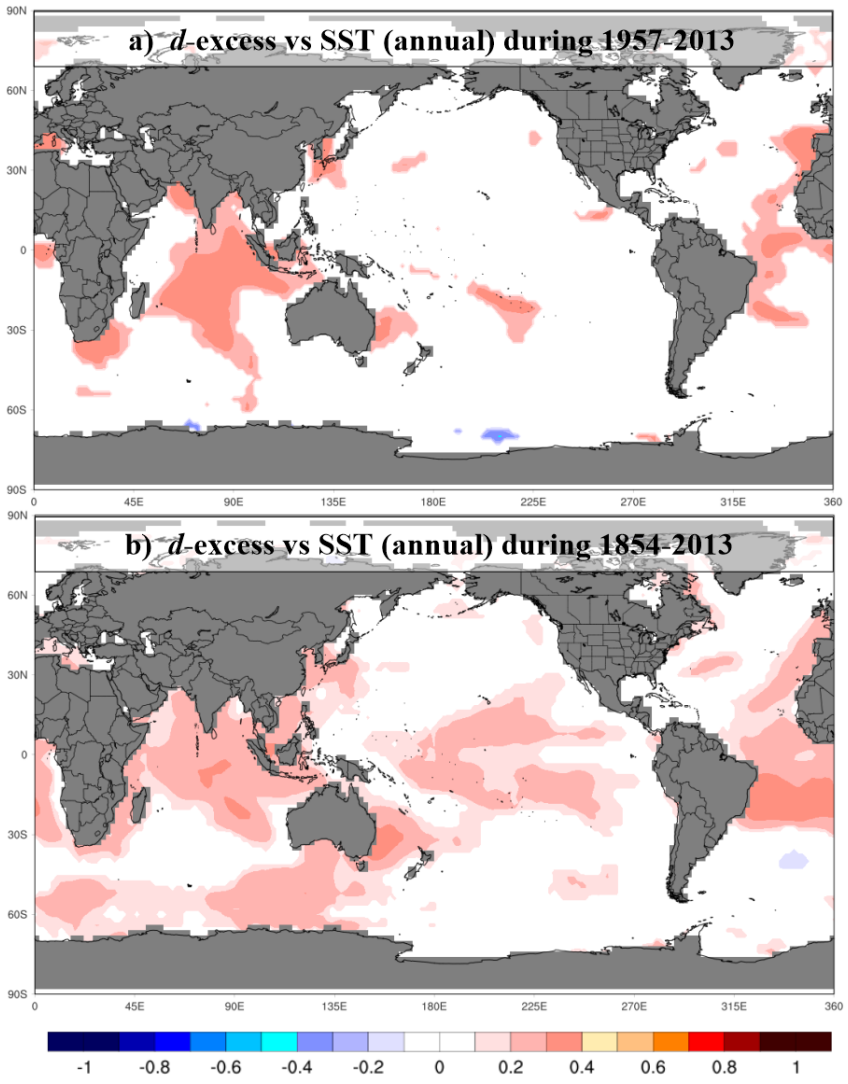


Figure 5. Spatial correlation of d-excess with annual sea surface temperature (SST) variability for (a) 1957–2013 CE and (b) 1854–2013 CE. The color bar indicates Pearson's correlation coefficient (r); only correlations significant at $p < 0.05$ are shown. This figure was generated using Climate Reanalyzer (https://climatereanalyzer.org/), Climate Change Institute, University of Maine, USA.

3.4 Discussion and implications

SA in the GV7-C ice core showed strong interannual variability and only a weak correlation with the IOD for 1957–2013 CE (Table 4). The IO and the western PO were identified as the moisture-source regions, together contributing approximately 87% of snowfall at the GV7 site, with the western PO accounting for 58% (147 mm) of total snowfall (Caiazzo et al., 2017). This likely indicates an influence of IO variability on SA at the GV7-C site. It was also reported that snowfall from the western PO sector was associated with a few intense snowfall events (Caiazzo et al., 2017). The variability in SA of the GV7-C ice core is therefore likely to be affected by the combined influence of large-scale atmospheric circulation, moisture-transport pathways, and transport efficiency, as well as short-lived synoptic-scale events such as intense precipitation associated with atmospheric rivers (Thomas et al., 2008; Cohen et al., 2013; Turner et al., 2019; Udy et al., 2021; Wille et al., 2021). Such processes are particularly important for Antarctic coastal snowfall and have been identified in ice-core records from coastal regions (Servettaz et al., 2020; Jackson et al., 2023). Moreover, the intensity and frequency of cyclone events affect snowfall in Antarctic coastal areas (Dalaiden et al., 2020a). In particular, in the Ross Sea region, cyclonically driven SA is dominant, and the region is sensitive to tropical and local climate drivers (Bertler et al., 2018). The contribution of synoptic-scale transport has been reported to be large for Victoria Land based on simulations over 1985–2014 CE (Dalaiden et al., 2020a). The influence of ENSO on SA was evident at the Law Dome site (Roberts et al., 2015). Atmospheric rivers can generate extreme snowfall and pronounced isotopic anomalies over Antarctica, potentially contributing disproportionately to the isotope signals preserved in ice cores (Wille et al., 2021; Dutrievoz et al., 2026). Wille et al. (2021) estimated that atmospheric rivers contribute approximately 10–20% of annual snowfall across broad regions of East Antarctica and can substantially influence interannual snowfall variability. Based on the lower-bound estimate of a 10% contribution, we applied a 10% increase to the mean annual accumulation of the GV7-C ice core, yielding a threshold value of 245 mm w.e. yr^{-1}. Years exceeding this value were classified as high-accumulation years. The mean summer-maximum $\delta^{18}O$ value during these high-accumulation years was −28.23 ± 1.70‰ (n = 83), compared with −28.71 ± 1.63‰ (n = 149) during the remaining years, representing a statistically significant enrichment of 0.48‰ ($p = 0.037$) in $\delta^{18}O$ during high-accumulation years. Similarly, the mean DJF $\delta^{18}O$ value was higher during high-accumulation years (–28.40 ± 1.69‰, n = 196) than during the remaining years (–28.81 ± 1.60‰, n = 251). These results suggest that years with higher snowfall accumulation may be associated with increased contributions from atmospheric-river events. We acknowledge that the contribution of atmospheric rivers to snowfall and associated $\delta^{18}O$ variability at the GV7-C site merits further investigation.

Given the correlations of $\delta^{18}O$ in the GV7-C ice core with Niño3.4, SOI, SAM, and SIE-RA for 1957–2013 CE (Fig. 3), the increase (decrease) in $\delta^{18}O$ can be partly explained by the intrusion of warm (cold) and moist (dry) air masses, mainly through the PO sector of the Southern Ocean. This suggests that ENSO- and SAM-related atmospheric circulation variability may modulate the transport of air masses from the PO sector toward the GV7-C site, contributing to the observed $\delta^{18}O$ variability. This finding is comparable to those from other ice cores in coastal Antarctica. In the Mount Brown South ice core in East Antarctica, evidence for moisture transport from the southern IO has been detected in the $\delta^{18}O$ signal, and extreme precipitation

events are linked to mid-latitude high-pressure systems that increase the transport of warm and moist air masses from the southern IO (Jackson et al., 2023). In another ice core from Adélie Land covering 1946–2006 CE, decadal variations in $\delta^{18}O$ and regional temperature were correlated, and $\delta^{18}O$ tended to decrease with increasing wind speed (Goursaud et al., 2017). However, $\delta^{18}O$ at the annual scale could not be explained by changes in SIE and temperature, indicating the importance of site-dependent climate signals in coastal ice cores (Goursaud et al., 2017). In another study, isotope-based results indicated colder SSTs, greater SIE, stronger katabatic winds, and decreasing SA in the Victoria Lower Glacier ice core during 1288–1807 CE (the Little Ice Age) (Bertler et al., 2011). Little Ice Age-related cooling is also evident in the $\delta^{18}O$ signal from the Hercules Névé ice core for 1770–1890 CE (Stenni et al., 1999) and in the frequent cold intervals of the Talos Dome ice core (Stenni et al., 2002). In line with these observations, a slight decreasing trend was observed in the $\delta^{18}O$ signal from the GV7-C ice core during 1782–1845 CE (Fig. 2), which may be part of Little Ice Age cooling. After 1845 CE, there was no long-term trend in $\delta^{18}O$ in the GV7-C ice core; rather, values lower than the long-term mean were frequently observed (blue arrows in Fig. 2). This depletion of $\delta^{18}O$ in the GV7-C ice core may be linked to changes in atmospheric circulation (e.g., SAM-related cooling) (Thompson and Solomon, 2002). Moreover, in terms of temperature reconstruction, the $\delta^{18}O$ signal in the GV7-C ice core contrasts with anthropogenic global warming, suggesting a stronger influence of local/regional variability or of various other climatic factors.

Given the correlations of d-excess with SST-SEIO and SST-SH (Tables 4 and 6), the d-excess signal from the GV7-C ice core is likely to preserve thermodynamic changes (i.e., SST changes), particularly over the IO sector of the Southern Ocean. Notably, the southern IO exhibits the most intense cyclonic activity in the Southern Ocean (Simmonds et al., 2003), which may enhance the detectability of this signal in the d-excess record. D-excess is an indicator of climate conditions in the source region (Jouzel et al., 1982; Sodemann and Stohl, 2009; Lewis et al., 2013); for example, warming over the Southern Ocean was found to co-vary with higher d-excess in the Victoria Lower Glacier ice core (Bertler et al., 2011). At the Law Dome ice-core site, d-excess also reflects SST changes over the southern IO sector (Masson-Delmotte et al., 2003). In particular, the abrupt increase in d-excess at Law Dome in the 1970s is consistent with that in the GV7-C ice core. This increase was attributed to abrupt changes in meridional atmospheric circulation, which led to the intrusion of warm subtropical moisture to the Antarctic coast during the 1970s (Masson-Delmotte et al., 2003). Large excursions (both high and low values) in the three-year running-averaged d-excess time series were more frequent after 1845 CE (Fig. 2). Furthermore, the warming phases of global average temperature during 1910–1945 CE and since 1976 CE (IPCC, 2001) are evident as increasing trends in d-excess (Fig. 2). Changes in SAM have also been linked to tropical SST changes and other tropical variability (Ding et al., 2012; Clem and Fogt, 2013). The climate signals at some coastal sites, including RICE, Mt. Erebus Saddle, and Styx Glacier, have been thought to be primarily indicative of local and regional conditions in the Ross Sea region (Rhodes et al., 2012; Nyamgerel et al., 2020, 2024). In addition, the influence of the IOD on precipitation over eastern East Antarctica was more dominant than SAM-induced changes for 1979–2014 CE (Lee and Jin, 2024). The IOD-related variation in precipitation is explained by waves originating from the IO that propagate southeastward and induce a low-pressure anomaly near eastern East Antarctica, consequently reducing

precipitation. Thus, at the GV7-C site, variability linked to remote teleconnections with SST over the IO sector of the Southern Ocean is assumed to be associated with d-excess.

Based on the various correlation analyses with the climate variables used in this study, our interpretations can be summarized as follows. During 1957–2013 CE, the correlation patterns of SA, $\delta^{18}O$, and d-excess suggest that snow precipitating at the GV7-C site mainly originates from the Southern Ocean, possibly via the western PO and southeastern IO sectors. For the longer period (1872–2013 CE), the correlation patterns between d-excess and SST indicate greater detectability of air-mass intrusion from the IO sector of the Southern Ocean. This suggests that warmer (colder) ocean surface conditions would be preserved as higher (lower) $\delta^{18}O$ (recent period) and d-excess values (recent and longer periods) in the GV7-C ice core. We note that three-year smoothing was used to examine persistent or low-frequency variability in the GV7-C ice-core records and their relationships with large-scale climate modes. The ice-core records integrate signals from multiple influencing factors, which may reinforce, weaken, or obscure one another. Therefore, correlations after smoothing are likely to reflect an averaged climate signal and may also represent the signal-preservation characteristics of the GV7-C ice core. Accordingly, the results are interpreted cautiously as indicating the dominant or more detectable component of multi-year climate variability recorded in the ice core. Moreover, the correlations discussed for the 1957–2013 CE and 1872–2013 CE periods represent relationships averaged over the respective study periods and may vary over time. Temporal variations in such relationships have been reported (Jouzel et al., 1997; Turner et al., 2020; Casado et al., 2026; Udy et al., 2026), and we acknowledge that further investigation using sub-period correlation analyses would help to better assess their temporal stability and evolution.

Finally, the GV7-C ice-core records constitute a valuable archive for investigating past climate variability. Historical temperature variability over the tropical oceans is important for global warming scenarios (IPCC, 2019). Projections show oceanic and atmospheric warming (Timmermann and Hellmer, 2013), and heat transported by the Southern Ocean further induces the melting of Antarctic ice shelves (Rignot et al., 2019). In particular, the IO is experiencing the strongest and most robust warming (Du and Xie, 2008; Beal et al., 2019), largely driven by anthropogenic forcing (Dong et al., 2014), and it is projected to warm non-uniformly (Sharma et al., 2023). Temperature anomalies over the IO and PO affect surface air temperature over Antarctica (Zhang and Duan, 2023). Moreover, warm SSTs in the western tropical IO excite a poleward-propagating Rossby wave, inducing changes in SIE (Zhang et al., 2024). Coastal and inland Antarctic regions have experienced anomalous sea-ice retreat and warming due to short-term intrusions of warm and moist air masses associated with a strongly negative SAM phase (Ionita et al., 2018). Recent SAM variability is unprecedented over the last millennium (Fogt and Marshall, 2020), and an increasing influence of SAM–ENSO coupling since the 1940s has been reported in coastal Dronning Maud Land (Ejaz et al., 2022). Thus, understanding the response of the Antarctic climate to ocean variability, particularly in the IO sector, is important for better assessing past and future Antarctic climate variability. In this context, the GV7-C ice-core record provides a valuable proxy for investigating the links between oceanic variability, atmospheric circulation, and Antarctic precipitation and isotope variability.

4 Conclusions

The $\delta^{18}O$, d-excess, and SA records from the GV7-C ice core in East Antarctica (1782–2013 CE) were analyzed to investigate potential links with large-scale climate variability. SA shows strong interannual variability, likely reflecting the combined influence of moisture-transport pathways, synoptic events, and local processes, and is only weakly correlated with SST variability over the IO for 1957–2013 CE. In contrast, $\delta^{18}O$ and d-excess exhibit detectable relationships with climate indices for 1957–2013 CE, including Niño3.4, SOI, SAM, the IOD, SST-SEIO, and reconstructed sea ice extent over the Ross–Amundsen Sea and East Antarctic sectors. Notably, d-excess shows a persistent relationship with SST-SEIO. Over the longer period (1872–2013 CE), the relationships of $\delta^{18}O$ with these indices generally weaken, suggesting time-varying controls, whereas d-excess retains its correlation with SST-SEIO. Correlation patterns and spatial analyses suggest that moisture reaching GV7-C primarily originates from the Southern Ocean, with contributions from the western PO and southeastern IO sectors during 1957–2013 CE, while the IO-sector influence is more evident over the longer period. Overall, the GV7-C record provides evidence for potential teleconnections between low-latitude ocean variability and coastal East Antarctic climate.

Code and data availability. Data reported in this study have been deposited at the Korea Polar Data Center (KPDC). Stable water isotope composition of the shallow ice core drilled at the GV7 site in 2013-2014. Dating the ice core/Paleoclimate research (https://dx.doi.org/doi:10.22663/KOPRI-KPDC-00000654). Climate Reanalyzer (https://climatereanalyzer.org/) from the Climate Change Institute, University of Maine, US, is publicly available.

Author contributions. YN: Conceptualization, Data analysis, Writing – original draft, Review and editing. YH: Conceptualization, Data analysis, Review and editing. SDH: Conceptualization, Review and editing. HK: Conceptualization, Review and editing. SK: Data analysis, Review and editing, JM: Data analysis, Review and editing, BS: Conceptualization, Review and editing, JL: Conceptualization, Review and editing.

Competing interests. The authors declare that they have no conflict of interest.

Financial support This work was supported by a Korea Polar Research Institute grant (PE26100) and a National Research Foundation of Korea grant funded by the Korean government (2022R1A2C3007047). This work was partially supported by Korea Institute of Marine Science & Technology Promotion (KIMST) funded by the Ministry of Oceans and Fishers (RS-2023-00256677; PM23020).

References

Beal, L.M., Vialard, J., Roxy, M.K., Ravichandran, N., McPhaden, M.J., Feng, M., Lumpkin, R., Unnikrishnan, A.S., Lee, M., Sloyan, B., Andres, M., Subramanian, A.C., Yu, L., Lengaigne, M., Shinoda, T., Annamalai, S., Ummenhofer, C.C., Strutton, P., Masumoto, Y., Tozuka, M., Wiggert, J., Han, W., and Hood, H.: IndOOS-2: a roadmap to sustained observations of the Indian Ocean for 2020–2030. CLIVAR-4/2019. https://doi.org/10.36071/clivar.rp.4-1.2019, 2019.

Bertler, N. A. N., Barrett, P. J., Mayewski, P. A., Fogt, R. L., Kreutz, K. J., and Shulmeister, J.: El Niño suppresses Antarctic warming, Geophys. Res. Lett., 31, L15207, doi:10.1029/2004GL020749, 2004.

Bertler, N.A.N, Mayewski, P., and Carter, L.: Cold conditions in Antarctica during the Little Ice Age – implications for abrupt climate change mechanisms. Earth and Planetary Science Letters, 308, 41–51, https://doi.org/10.1016/j.epsl.2011.05.021, 2011.

Bertler, N. A. N., Conway, H., Dahl-Jensen, D., Emanuelsson, D. B., Winstrup, M., Vallelonga, P. T., Lee, J. E., Brook, E. J., Severinghaus, J. P., Fudge, T. J., Keller, E. D., Baisden, W. T., Hindmarsh, R. C. A., Neff, P. D., Blunier, T., Edwards, R., Mayewski, P. A., Kipfstuhl, S., Buizert, C., Canessa, S., Dadic, R., Kjær, H. A., Kurbatov, A., Zhang, D., Waddington, E. D., Baccolo, G., Beers, T., Brightley, H. J., Carter, L., Clemens-Sewall, D., Ciobanu, V. G., Delmonte, B., Eling, L., Ellis, A., Ganesh, S., Golledge, N. R., Haines, S., Handley, M., Hawley, R. L., Hogan, C. M., Johnson, K. M., Korotkikh, E., Lowry, D. P., Mandeno, D., McKay, R. M., Menking, J. A., Naish, T. R., Noerling, C., Ollive, A., Orsi, A., Proemse, B. C., Pyne, A. R., Pyne, R. L., Renwick, J., Scherer, R. P., Semper, S., Simonsen, M., Sneed, S. B., Steig, E. J., Tuohy, A., Venugopal, A. U., Valero-Delgado, F., Venkatesh, J., Wang, F., Wang, S., Winski, D. A., Winton, V. H. L., Whiteford, A., Xiao, C., Yang, J., and Zhang, X.: The Ross Sea dipole – temperature, snow accumulation and sea ice variability in the Ross Sea region, Antarctica, over the past 2700 years. Climate of the Past, 14, 193–214. https://doi.org/10.5194/cp-14-193-2018, 2018.

Bretherton, C. S., Widmann, M., Dymnikov, V. P., Wallace, J. M. and Bladé, I.: The effective number of spatial degrees of freedom of a time-varying field. J. Clim. 12, 1990–2009. https://doi.org/10.1175/1520-0442(1999)012<1990:TENOSD>2.0.CO;2, 1999.

Caiazzo, L., Baccolo, G., Barbante, C., Becagli, S., Berto, M., Ciardini, V., Crotti, I., Delmonte, B., Dreossi, G., Frezzotti, M., Gabrieli, J., Giardi, F., Han, Y., Hong, S-B., Hur, S.D., Hwang, H., Kang, J-H., Narcisi, B., Proposito, M., Scarchilli, C., Selmo, E., Severi, M., Spolaor, A., Traversi, R., and Udisti, R.: Prominent features in isotopic, chemical and dust stratigraphies from coastal East Antarctic ice sheet (Eastern Wilkes Land). Chemosphere, 176, 273-287. https://doi.org/10.1016/j.chemosphere.2017.02.115, 2017.

Casado, M., Bailey, A., Leroy-Dos Santos, C., Fourré,E., Favier, V., Agosta, C., Dutrievoz, N., Kittel, C., Arnaud, L., Prié, F., Akers, P.D., Cauquoin, A., Werner, M., Janssen, L., Stenni, B., Dreossi, G., Spolaor, A., Petteni, A.,Savarino, J., and Landais, A.: Water isotope–temperature relationship variability across Antarctica set by atmospheric circulation. Nat. Geosci. 19, 581–588. https://doi.org/10.1038/s41561-026-01961-y, 2026.

Caton Harrison, T., Biri, S., Bracegirdle, T. J., King, J. C., Kent, E. C., Vignon, É., and Turner, J.: Reanalysis representation of low-level winds in the Antarctic near-coastal region, Weather Clim. Dynam., 3, 1415–1437, https://doi.org/10.5194/wcd-3-1415-2022, 2022.

Clem, K. R., and Fogt, R. L.: Varying roles of ENSO and SAM on the Antarctic Peninsula climate in austral spring. Journal of Geophysical Research: Atmospheres, 118(20), 11,481–11,492. https://doi.org/10.1002/jgrd.50860, 2013.

Cohen, L., Dean, S., and Renwick, J.: Synoptic Weather Types for the Ross Sea Region, Antarctica. J. Climate, 26, 636–649, https://doi.org/10.1175/JCLI-D-11-00690.1, 2013.

Constable, A.J., Harper,S., Dawson, J., Holsman, K., Mustonen, T., Piepenburg, D., and Rost, B.: Cross-Chapter Paper 6: Polar Regions. In: Climate Change 2022: Impacts, Adaptation and Vulnerability. Contribution of Working Group II to the Sixth Assessment Report of the Intergovernmental Panel on Climate Change [H.-O. Pörtner, D.C. Roberts, M. Tignor,E.S. Poloczanska, K. Mintenbeck, A. Alegría, M. Craig, S. Langsdorf, S. Löschke, V. Möller, A. Okem, B. Rama (eds.)].Cambridge University Press, Cambridge, UK and New York, NY, USA, pp. 2319–2368, doi:10.1017/9781009325844.023, 2022.

Craig, H.: Isotopic variations in meteoric waters. Science, 133, 1702–1703. DOI: 10.1126/science.133.3465.1702, 1961.

Dalaiden, Q., Goosse, H., Lenaerts, J.T.M., Cavitte, M.G.P., and Henderson, N.: Future Antarctic snow accumulation trend is dominated by atmospheric synoptic-scale events. Communications Earth & Environment, 1, 62. https://doi.org/10.1038/s43247-020-00062-x, 2020a.

Dalaiden, Q., Goosse, H., Klein, F., Lenaerts, J. T. M., Holloway, M., Sime, L., and Thomas, E.R.: How useful is snow accumulation in reconstructing surface air temperature in Antarctica? A study combining ice core records and climate models, The Cryosphere, 14, 1187–1207, https://doi.org/10.5194/tc-14-1187-2020, 2020b.

Delmotte, M., Masson, V., Jouzel J, and Morgan, V.: A seasonal deuterium excess signal at Law Dome, coastal Eastern Antarctica: a Southern Ocean signature. Journal of Geophysical Research 105(D6): 7187–7197, 2000.

Ding, Q., Steig, E. J., Battisti, D. S., and Wallace, J. M.: Influence of the tropics on the Southern Annular Mode. Journal of Climate, 25 (18), 6330–6348. https://doi.org/10.1175/JCLI-D-11-00523.1, 2012.

Divine, D. V., E. Isaksson, M. Kaczmarska, F. Godtliebsen, H. Oerter, E. Schlosser, S. J. Johnsen, M. van den Broeke, and R. S. W. van de Wal.: Tropical Pacific–high latitude south Atlantic teleconnections as seen in $\delta^{18}O$ variability in Antarctic coastal ice cores, J. Geophys. Res., 114, D11112, doi:10.1029/2008JD010475, 2009.

Dong, L., Zhou, T., and Wu, B.: Indian Ocean warming during 1958–2004 simulated by a climate system model and its mechanism. Clim Dyn 42, 203–217. https://doi.org/10.1007/s00382-013-1722-z, 2014.

Du, Y., and Xie, S.-P.: Role of atmospheric adjustments in the tropical Indian Ocean warming during the 20th century in climate models. Geophysical Research Letters, 35(8), Article L08712. https://doi.org/10.1029/2008GL033631, 2008.

Dutrievoz, N., Agosta, C., Davrinche, C., Landais, A., Nguyen, S., Vignon, É., Ollivier, I., Leroy-Dos Santos, C., Fourré, E., Casado, M., Wille, J., Favier, V., Minster, B., and Prié, F.: Water vapour isotope anomalies during an atmospheric river event at Dome C, East Antarctica. The Cryosphere, 20, 1025–1046, 2026.

Ejaz, T., Rahaman, W., Laluraj, C.M., Mahalinganathan, K., and Thamban, M.: Rapid Warming Over East Antarctica Since the 1940s Caused by Increasing Influence of El Niño Southern Oscillation and Southern Annular Mode. Front. Earth Sci. 10:799613. doi: 10.3389/feart.2022.799613, 2022.

Ekaykin, A.A., Lipenkov, V.Ya., Kuzmina, I.N., Petit, J.R., Masson-Delmotte, V., Johnsen, S.J.: The changes in isotope composition and accumulation of snow at Vostok station, East Antarctica, over the past 200 years. Annals of Glaciology. 2004;39:569-575. doi:10.3189/172756404781814348

Fogt, R. L., Wovrosh, A. J., Langen, R. A., and Simmonds, I.: The characteristic variability and connection to the underlying synoptic activity of the Amundsen-Bellingshausen Seas Low. Journal of Geophysical Research, 117, D07111. doi:10.1029/2011JD017337, 2012.

Fogt, R.L., and Marshall GJ.: The Southern Annular Mode: Variability, trends, and climate impacts across the Southern Hemisphere. WIREs Clim Change. 2020; 11:e652. https://doi.org/10.1002/wcc.652, 2020.

Fogt, R. L., Raphael, M. N., and Handcock, M.S.: Seasonal Antarctic Sea Ice Extent Reconstructions, 1905-2020, Version 1. [East Antarctica and Ross-Amundsen reconstruction ensembles]. Boulder, Colorado USA. NSIDC:National Snow and Ice Data Center. https://doi.org/10.7265/55x7-we68, 2023.

Fretwell, P., Pritchard, H. D., Vaughan, D. G., Bamber, J. L., Barrand, N. E., Bell, R., Bianchi, C., Bingham, R. G., Blankenship, D. D., Casassa, G., Catania, G., Callens, D., Conway, H., Cook, A. J., Corr, H. F. J., Damaske, D., Damm, V., Ferraccioli, F., Forsberg, R., Fujita, S., Gim, Y., Gogineni, P., Griggs, J. A., Hindmarsh, R. C. A., Holmlund, P., Holt, J. W., Jacobel, R. W., Jenkins, A., Jokat, W., Jordan, T., King, E. C., Kohler, J., Krabill, W., Riger-Kusk, M., Langley, K. A., Leitchenkov, G., Leuschen, C., Luyendyk, B. P., Matsuoka, K., Mouginot, J., Nitsche, F. O., Nogi, Y., Nost, O. A., Popov, S. V., Rignot, E., Rippin, D. M., Rivera, A., Roberts, J., Ross, N., Siegert, M. J., Smith, A. M., Steinhage, D., Studinger, M., Sun, B., Tinto, B. K., Welch, B. C., Wilson, D., Young, D. A., Xiangbin, C., and Zirizzotti, A.: Bedmap2: improved ice bed, surface and thickness datasets for Antarctica, The Cryosphere, 7, 375–393, https://doi.org/10.5194/tc-7-375-2013.

Frezzotti, M., Urbini, S., Proposito, M., Scarchilli, C., and Gandolfi, S.: Spatial and temporal variability of surface mass balance near Talos Dome, East Antarctica. Journal of Geophysical Research, 112, F02032. https://doi.org/10.1029/2006JF000638, 2007.

Frieler, K., Clark, P., He, F., Buizert, C., Reese, R., Ligtenberg, S.R.M., van den Broeke, M.R., Winkelmann, R., and Levermann, A.: Consistent evidence of increasing Antarctic accumulation with warming. Nature Climate Change, 5, 348–352. https://doi.org/10.1038/nclimate2574, 2015.

Goursaud, S., Masson-Delmotte, V., Favier, V., Preunkert, S., Fily, M., Gallée, H., Jourdain, B., Legrand, M., Magand, O., Minster, B., and Werner, M.: A 60-year ice-core record of regional climate from Adélie Land, coastal Antarctica. The Cryosphere, 11, 343–362. doi: 10.5194/tc-11-343-2017, 2017.

Goursaud, S., Masson-Delmotte, V., Favier, V., Preunkert, S., Legrand, M., Minster, B., and Werner, M.: Challenges associated with the climatic interpretation of water stable isotope records from a highly resolved firn core from Adélie Land, coastal Antarctica. The Cryosphere, 13, 1297–1324. https://doi.org/10.5194/tc-13-1297-2019, 2019.

Hall, A., and Visbeck, M.: Synchronous variability in the southern hemisphere atmosphere, sea ice, and ocean resulting from the annular mode. Journal of Climate, 15: 3043–3057. https://doi.org/10.1175/1520-0442(2002)015<3043:SVITSH>2.0.CO;2, 2002.

Hersbach, H., Bell, B., Berrisford, P., Hirahara, S., Horányi, A., Muñoz-Sabater, J., Nicolas, J., Peubey, C., Radu, R., Schepers, D., Simmons, A., Soci, C., et al.:The ERA5 global reanalysis. Quarterly Journal of the Royal Meteorological Society, 146(730), 1999–2049. https://doi.org/10.1002/qj.3803, 2020.

Huang, B., Thorne, P.W., Banzon, V.F., Boyer, T., Chepurin, G., Lawrimore, J.H., Menne, M.J., Smith, T.M., Vose, R.S., and Zhang, H-M.: NOAA Extended Reconstructed Sea Surface Temperature (ERSST), Version 5. [Southern Hemisphere Ocean Temperature Anomalies]. NOAA National Centers for Environmental Information. doi:10.7289/V5T72FNM, 2017.

Ionita, M., Scholz, P., Grosfeld, K., and Treffeisen, R.: Moisture transport and Antarctic sea ice: austral spring 2016 event, Earth Syst. Dynam., 9, 939–954, https://doi.org/10.5194/esd-9-939-2018, 2018.

IPCC, 2001: Climate Change 2001: The Scientific Basis. Contribution of Working Group I to the Third Assessment Report of the Intergovernmental Panel on Climate Change [Houghton, J.T.,Y. Ding, D.J. Griggs, M. Noguer, P.J. van der Linden, X. Dai, K. Maskell, and C.A. Johnson (eds.)]. Cambridge University Press, Cambridge, United Kingdom and New York, NY, USA, 881pp.

IPCC, 2019: Technical Summary [H.-O. Pörtner, D.C. Roberts, V. Masson-Delmotte, P. Zhai, E. Poloczanska, K. Mintenbeck, M. Tignor, A. Alegría, M. Nicolai, A. Okem, J. Petzold, B. Rama, N.M. Weyer (eds.)]. In: IPCC Special Report on the Ocean and Cryosphere in a Changing Climate [H.- O. Pörtner, D.C. Roberts, V. Masson-Delmotte, P. Zhai, M. Tignor, E. Poloczanska, K. Mintenbeck, A. Alegría, M. Nicolai, A. Okem, J. Petzold, B. Rama, N.M. Weyer (eds.)]. In press.

Jackson, S. L., Vance, T. R., Crockart, C., Moy, A., Plummer, C., and Abram, N. J.: Climatology of the Mount Brown South ice core site in East Antarctica: implications for the interpretation of a water isotope record. Climate of the Past, 19, 1653–1675. https://doi.org/10.5194/cp-19-1653-2023, 2023.

Jouzel, J., Merlivat, L., and Lorius, C.: Deuterium excess in an East Antarctic ice core suggests higher relative humidity at the oceanic surface during the last glacial maximum. Nature, 299, 688–691. https://www.nature.com/articles/299688a0, 1982.

Jouzel, J., Alley, R. B., Cuffey, K. M., Dansgaard, W., Grootes, P., Hoffmann, G., Johnsen, S.J., Koster, R.D., Peel, D., Shuman, C.A., Stievenard, M., Stuiver, M., and White, J.: Validity of the temperature reconstruction from water isotopes in ice cores. Journal of Geophysical Research Oceans, 102, 26471–26487, https://doi.org/10.1029/97JC01283, 1997.

Khan. I. (2019). Climate-related variability of isotopic records in a coastal Antarctic ice (Master's thesis). Retrieved from [http://hdl.handle.net/10579/15637]. Venice, Italy: Università Ca' Foscari Venezia.

Kim, BH., Seo, KW., Eom, J., Chen, J., and Wilson., C.: Antarctic ice mass variations from 1979 to 2017 driven by anomalous precipitation accumulation. Scientific Reports, 10, 20366. https://doi.org/10.1038/s41598-020-77403-5, 2020.

Kim, J., Kang, D., Lee, M.-I., Jin, E. K., Kug, J.-S., and Lee, W. S. (2023). Remote influences of ENSO and IOD on the interannual variability of the West Antarctic sea ice. Journal of Geophysical Research: Atmospheres, 128, e2022JD038313. https://doi.org/10.1029/2022JD038313

Kim, S., Han, Y., Chung, J., Ro, S., Moon, J., Hur, S. D., and Lee, J.: Imprints of sea ice, wind patterns, and atmospheric systems on summer water isotope signatures at Hercules Névé, East Antarctica, The Cryosphere, 19, 5655–5670, https://doi.org/10.5194/tc-19-5655-2025, 2025.

Kino, K., Okazaki, A., Cauquoin, A., and Yoshimura, K.: Contribution of the Southern Annular Mode to variations in water isotopes of daily precipitation at Dome Fuji, East Antarctica. Journal of Geophysical Research: Atmospheres, 126, e2021JD035397. https://doi. org/10.1029/2021JD035397, 2021.

Klein, F., Abram, N. J., Curran, M. A. J., Goosse, H., Goursaud, S., Masson-Delmotte, V., Moy, A., Neukom, R., Orsi, A., Sjolte, J., Steiger, N., Stenni, B., and Werner, M.: Assessing the robustness of Antarctic temperature reconstructions over the past 2 millennia using pseudoproxy and data assimilation experiments, Climate of the Past, 15, 661–684. https://doi.org/10.5194/cp-15-661-2019, 2019.

Lee, H-J., and Jin, E.M.: The dominant influence of indian ocean dipole-like ocean warming on decreased precipitation over eastern East Antarctica. Front. Earth Sci. 12:1387809. doi: 10.3389/feart.2024.1387809, 2024.

Leroy-Dos Santos, C., Fourré, E., Agosta, C., Casado, M., Cauquoin, A., Werner, M., Minster, B., Prié, F., Jossoud, O., Petit, L., and Landais, A.: From atmospheric water isotopes measurement to firn core interpretation in Adélie Land: a case study for isotope-enabled atmospheric models in Antarctica. The Cryosphere, 17, 5241–5254. https://doi.org/10.5194/tc-17-5241-2023, 2023.

Lewis, S.C., LeGrande, A.N., Kelley, M., and Schmidt, G.A.: Modeling insights into deuterium excess as an indicator of water vapor source conditions. J. Geophys. Res. Atmos., 118, no. 2, 243-262, doi:10.1029/2012JD017804, 2013.

Liu H., Jezek K.C., Li B. and Zhao Z.: Radarsat Antarctic Mapping Project Digital Elevation Model, Version 2. Boulder, Colorado USA. NASA National Snow and Ice Data Center Distributed Active Archive Center. doi: 10.5067/8JKNEW6BFRVD, 2015.

Magand, O., Frezzotti, M., Pourchet, M., Stenni,B., Genoni, L., and Fily, M.: Climate variability along latitudinal and longitudinal transects in east Antarctica. Annals of Glaciology, 39, 351–358. doi:10.3189/172756404781813961, 2004.

Markle, B. R., and Steig, E. J.: Improving temperature reconstructions from ice-core water-isotope records. Climate of the Past, 18, 1321–1368. https://doi.org/10.5194/cp-18-1321-2022, 2022.

Marshall, G.: Trends in the Southern annular mode from observations and reanalyses. Journal of Climate, 16(24), 4134–4143. https://doi.org/10.1175/1520-0442(2003)016<4134:Titsam>2.0.Co;2, 2003

Marshall, G. J., & National Center for Atmospheric Research Staff (Eds.). (2018). The Climate Data Guide: Marshall Southern Annular Mode (SAM) Index (Station-based). Retrieved from https://climatedataguide.ucar.edu/climate-data/marshall-southern-annular-mode-sam-index-station-based

Marshall, G.J., Fogt, R.L., Turner, J. et al.: Can current reanalyses accurately portray changes in Southern Annular Mode structure prior to 1979?. Clim Dyn 59, 3717–3740 (2022). https://doi.org/10.1007/s00382-022-06292-3, 2022

Masson-Delmotte, V., Delmotte, M., Morgan, V., Etheridge, D., van Ommen, T., Tartarin, S., and Hoffmann, G.: Recent southern Indian Ocean climate variability inferred from a Law Dome ice core: new insights for the interpretation of coastal Antarctic isotopic records. Climate Dynamics 21, 153–166. https://doi.org/10.1007/s00382-003-0321-9, 2003.

Masson-Delmotte, V. S., Hou, S., Ekaykin, A., Jouzel, J., Aristarain, A., Bernardo, R.T., Bromwich, D., Cattani, O., Delmotte, M., Falourd, S., Frezzotti, M., Gallée, H., Genoni, L., Isaksson, E., Landais, A., Helsen, M.M., Hoffmann, G., Lopez, J., Morgan, V., Motoyama, H., Noone, D., Oerter, H., Petit, J.R., Royer, A., Uemura, R., Schmidt, G.A., Schlosser, E., Simões, J.C., Steig, E.J., Stenni, B., Stievenard, M., van den Broeke, M.R., van de Wal, R.S.W., van de Berg, W.J., Vimeux, F., and White, J.W.C.: A review of Antarctic surface snow isotopic composition: Observations, atmospheric circulation, and isotopic modeling. Journal of Climate, 21, 3359-3387. doi:10.1175/2007JCLI2139.1, 2008.

Matsuoka, K., Skoglund, A., Roth, G., de Pomereu, J., Griffiths, H., and Headland, R.: Quantarctica, an integrated mapping environment for Antarctica, the Southern Ocean, and sub-Antarctic islands. Environmental Modelling & Software 140, 105015. doi:10.1016/j.envsoft.2021.105015, 2021.

Mayewski, P. A., Meredith, M.P., Summerhayes, C.P., Turner, J., Worby, A., Barrett, J., Casassa, G., Bertler, N.A.N., Bracegirdle, A.C., Garabato, N., Bromwich, D., Campbell, H., Hamilton, G.S., Lyons, W.B., Maasch, K.A., Aoki, S., Xiao, C., and Tas van Ommen.: State of the Antarctic and Southern Ocean climate system, Rev. Geophys., 47, RG1003, doi:10.1029/2007RG000231, 2009.

Medley, B., McConnell, J. R., Neumann, T. A., Reijmer, C. H., Chellman, N., Sigl, M., and Kipfstuhl, S.: Temperature and Snowfall in Western Queen Maud Land Increasing Faster Than Climate Model Projections. Geophysical Research Letters, 45, 1472–1480. https://doi.org/10.1002/2017GL075992, 2018.

Meyerson, E.A., Mayewski, P.A., Kreutz, K.J., David Meeker, L., Whitlow, S.I, and Twickler, M.S.: The polar expression of ENSO and sea-ice variability as recorded in a South Pole ice core. Annals of Glaciology, 2002;35:430-436. doi:10.3189/172756402781817149, 2002.

Nardin, R., Severi, M., Amore, A., Becagli, S., Burgay, F., Caiazzo, L., Ciardini, V., Dreossi, G., Frezzotti, M., Hong, S.-B., Khan, I., Narcisi, B. M., Proposito, M., Scarchilli, C., Selmo, E., Spolaor, A., Stenni, B., and Traversi, R.: Dating of the GV7 East Antarctic ice core by high-resolution chemical records and focus on the accumulation rate variability in the last millennium. Climate of the Past, 17, 2073–2089, https://doi.org/10.5194/cp-17-2073-2021, 2021.

Nicolas, J. P., and Bromwich, D. H.: New Reconstruction of Antarctic Near-Surface Temperatures: Multidecadal Trends and Reliability of Global Reanalyses, Journal of Climate, 27(21), 8070-8093. https://doi.org/10.1175/JCLI-D-13-00733.1, 2014.

Nyamgerel, Y., Han, Y., Kim, S., Hong, S., Lee, J., and Hur, S. Chronological characteristics for snow accumulation on Styx Glacier in northern Victoria Land, Antarctica. Journal of Glaciology, 66(260), 916-926. doi:10.1017/jog.2020.53, 2020.

Nyamgerel, Y., Hong, S.-B., Han, Y., Kim, S., Lee, J., and Hur, S. D.: Snow-pit record from a coastal Antarctic site and its preservation of meteorological features, Earth Interact., 25, 108–118, https://doi.org/10.1175/EI-D-20-0018.1, 2021.

Nyamgerel, Y., Han, Y., Hwang, H., Han, C., Hong, S., Hur, S., and Lee, J.: Climate-related variabilities in the Styx-M ice core record from northern Victoria Land, East Antarctica, during 1979–2014, Science of The Total Environment, 935, 173319, doi.org/10.1016/j.scitotenv.2024.173319, 2024.

Oerter, H., Wilhelms, F., Jung-Rothenhausler, F., Goktas, F., Miller, H., Graf, W., and Sommer, S.: Accumulation rates in Dronning Maud Land, Antarctica, as revealed by dielectric-profiling measurements of shallow firn cores. Annals of Glaciology, 30, 27–34, https://doi.org/10.3189/172756400781820705, 2000.

Palerme, C., Genthon, C., Claud, C., Kay, J.E., Wood, N.B., and L'Ecuyer, T.: Evaluation of current and projected Antarctic precipitation in CMIP5 models. Climate Dynamics, 48, 225–239. https://doi.org/10.1007/s00382-016-3071-1, 2017.

Pohl, B., Favier, V., Wille, J., Udy, D. G, Vance, T. R, Pergaud, J., Dutrievoz, N., Blanchet, J., Kittel, C., Amory, C., Krinner, G., Codron, F.: Relationship between weather regimes and atmospheric rivers in East Antarctica. Journal of Geophysical Research: Atmospheres, 126, e2021JD035294. https://doi.org/10.1029/2021JD035294, 2021.

Purich, A., England, M. H., Cai, W., Chikamoto, Y., Timmermann, A., Fyfe, J. C., Frankcombe, L., Meehl, G.A., and Arblaster, J.M.: Tropical Pacific SST Drivers of Recent Antarctic Sea Ice Trends. Journal of Climate, 29(24), 8931-8948, https://doi.org/10.1175/JCLI-D-16-0440.1, 2016.

Rayner N. A., D. E. Parker, E. B. Horton, C. K. Folland, L. V. Alexander, D. P. Rowell, E. C. Kent, A. Kaplan.; Global analyses of sea surface temperature, sea ice, and night marine air temperature since the late nineteenth century, J. Geophys. Res., 108 (D14), 4407, doi:10.1029/2002JD002670, 2003.

Rhodes, R. H., Bertler, N. A. N., Baker, J. A., Steen-Larsen, H. C., Sneed, S. B., Morgenstern, U., and Johnsen, S. J.: Little Ice Age climate and oceanic conditions of the Ross Sea, Antarctica from a coastal ice core record, Clim. Past, 8, 1223–1238, https://doi.org/10.5194/cp-8-1223-2012, 2012.

Rignot, E., Mouginot, J., Scheuchl, B., van den Broeke, M., van Wessem, M. J., and Morlighem, M.: Four decades of Antarctic Ice Sheet mass balance from 1979-2017. Proceedings of the National Academy of Sciences of the United States of America, 116(4), 1095–1103. https://doi.org/10.1073/pnas.1812883116, 2019.

Rintoul, S.R., Chown, S.L., DeConto, R.M., England, M.H., Fricker, H.A., Masson-Delmotte, V., Naish, T.R., Sieger, M.J., and Xavier, J.C.: Choosing the future of Antarctica. Nature 558, 233–241 (2018). https://doi.org/10.1038/s41586-018-0173-4, 2018.

Roberts, J., Plummer, C., Vance, T., van Ommen, T., Moy, A., and Poynter, S.: A 2000 year annual record of snow accumulation rates for Law Dome, East Antarctica. Climate of the Past, 11 (5). pp. 697-707. https://doi.org/10.5194/cp-11-697-2015, 2015.

Russell, A., and McGregor, G.R.: Southern hemisphere atmospheric circulation: impacts on Antarctic climate and reconstructions from Antarctic ice core data. Climatic Change, 99, 155–192. https://doi.org/10.1007/s10584-009-9673-4, 2010.

Schneider, D. P., and Steig, E. J.: Ice cores record significant 1940s Antarctic warmth related to tropical climate variability. Proc. Natl. Acad. Sci. U.S.A. 105, 12154–12158, 2008.

Schlosser, E., and Oerter, H.: Seasonal variations of accumulation and the isotope record in ice cores: a study with surface snow samples and firn cores from Neumayer station, Antarctica. Annals of Glaciology. 2002;35:97-101. doi:10.3189/172756402781817374, 2002.

Schlosser, E., H. Anschütz, D. Divine, T. Martma, A. Sinisalo, S. Altnau, and E. Isaksson.: Recent climate tendencies on an East Antarctic ice shelf inferred from a shallow firn core network, J. Geophys. Res. Atmos., 119, 6549–6562, doi:10.1002/2013JD020818, 2014.

Sodemann, H., and Stohl, A.: Asymmetries in the moisture origin of Antarctic precipitation. Geophysical Research Letters, 36, L22803, doi:10.1029/2009GL040242, 2009.

Servettaz, A. P. M., Orsi, A. J., Curran, M. A. J., Moy, A. D., Landais, A., Agosta, C., Holly, V., Winton, L., Touzeau, A., McConnell, J.R., Werner, M., and Baroni, M.: Snowfall and water stable isotope variability in East Antarctica controlled by warm synoptic events. Journal of Geophysical Research: Atmospheres, 125, e2020JD032863. https://doi.org/10.1029/2020JD032863, 2020.

Sharma, S., Ha, KJ., Yamaguchi, R., Rodgers, K.B., Timmermann, A., and Chung, E-S.: Future Indian Ocean warming patterns. Nat Commun 14, 1789 (2023). https://doi.org/10.1038/s41467-023-37435-7, 2023.

Simmonds, I., Keay, K., Lim, E-P.: Synoptic activity in the seas around Antarctica. Mon. Wea. Rev., 131, 272–288, https://doi.org/10.1175/1520-0493(2003)131<0272:SAITSA>2.0.CO;2, 2003.

Stenni, B., Caprioli, R., Cimino, L., Cremisini, C., Flora, O., Gragnani, R., Longinelli, A., Maggi, V., and Torcini, S.: Years of isotope and chemical records in a firn core from Hercules Névé, Northern Victoria Land, Antarctica. Annals of Glaciology, 29, 106–112. doi: 10.3189/172756499781821175, 1999.

Stenni, B., Masson-Delmotte, V., Johnsen, S., Jouzel, J., Longinelli, A., Monnin, E., Rothlisberger, R., and Selmo, E.: An oceanic cold reversal during the last deglaciation. Science. 2001 Sep 14;293(5537):2074-7. doi: 10.1126/science.1059702. PMID: 11557889, 2001.

Stenni, B., Proposito, M., Gragnani., R., Flora, O., Jouzel, J., Falourd, S., and Frezzotti, M.: Eight centuries of volcanic signal and climate change at Talos Dome (East Antarctica). Journal of Geophysical Research, 107(D9), 1–14. doi:10.1029/2000JD000317, 2002.

Stenni, B., Curran, M. A. J., Abram, N. J., Orsi, A., Goursaud, S., Masson-Delmotte, V., Neukom, R., Goosse, H., Divine, D., van Ommen, T., Steig, E. J., Dixon, D. A., Thomas, E. R., Bertler, N. A. N., Isaksson, E., Ekaykin, A., Werner, M., and Frezzotti, M.: Antarctic climate variability on regional and continental scales over the last 2000 years. Climate of the Past, 13, 1609–1634, https://doi.org/10.5194/cp-13-1609-2017, 2017.

Tetzner, D., Thomas, E., and Allen, C.: A Validation of ERA5 Reanalysis Data in the Southern Antarctic Peninsula—Ellsworth Land Region, and Its Implications for Ice Core Studies. Geosciences, 9(7), 289. https://doi.org/10.3390/geosciences9070289, 2019.

Thomas, E. R., Marshall, G. J., and McConnell, J. R.: A doubling in snow accumulation in the western Antarctic Peninsula since 1850. Geophysical Research Letters, 35, L01706, doi:10.1029/2007GL032529, 2008.

Thomas, E. R., and Abram, N. J.: Ice core reconstruction of sea ice change in the Amundsen-Ross Seas since 1702 A.D. Geophysical Research Letters, 43, 5309–5317, doi:10.1002/2016GL068130, 2016.

Thomas, E. R., Tetzner, D., Markle, B., Pedro, J., Gacitúa, G., Moser, D. E., and Jackson, S.: The first firn core from Peter I Island – capturing climate variability across the Bellingshausen Sea, Clim. Past, 20, 2525–2538, https://doi.org/10.5194/cp-20-2525-2024, 2024.

Thompson, D. and Solomon, S.: Interpretation of recent southern hemisphere climate change, Science, 296(5569), 895-899, 2002.

Timmermann, R., and Hellmer, H. H.: Southern Ocean warming and increased ice shelf basal melting in the twenty-first and twenty-second centuries based on coupled ice-ocean finite-element modelling. Ocean Dynamics, 63(9–10), 1011–1026. https://doi.org/10.1007/s10236-013-0642-0, 2013.

Tuohy, A., Bertler, N., Neff, P., Edwards, R., Emanuelsson, D., Beers, T., and Mayewski, P.: Transport and deposition of heavy metals in the Ross Sea Region, Antarctica, Journal of Geophysical. Research. Atmospheres, 120, 10,996– 11,011. doi:10.1002/2015JD023293, 2015.

Turner, J., R.A., Bindschadler, P., Convey, G., di Prisco, E., Fahrbach, J., Gutt, D.A., and Hodgson, P.A.: Mayewski and C.P. Summerhayes (editors). (2009). Antarctic climate change and the environment. Cambridge: Scientific Committee on Antarctic Research.

Turner, J., Phillips, T., Thamban, M., Rahaman, W., Marshall, G. J., Wille, J. D., Favier, V., Winton, V.H.L., Thomas, E., Wang, Z., van den Broeke, M., Hosking, J.S., and Lachlan-Cope, T.: The dominant role of extreme precipitation events in Antarctic snowfall variability. Geophysical Research Letters, 46, 3502–3511. https://doi.org/10.1029/2018GL081517, 2019.

Turner, J., Marshall, G. J., Clem, K., Colwell, S., Phillips, T., and Lu, H.: Antarctic temperature variability and change from station data. International Journal of Climatology, 40(6), 2986–3007. https://doi.org/10.1002/joc.6378, 2020.

Udy, D. G., T. R. Vance, A. S. Kiem, N. J. Holbrook, and M. A. J. Curran.: Links between Large-Scale Modes of Climate Variability and Synoptic Weather Patterns in the Southern Indian Ocean. J. Climate, 34, 883–899, https://doi.org/10.1175/JCLI-D-20-0297.1, 2021.

Udy, D., Jackson, S., Vance, T. R., Pohl, B., Kiem, A. S., Holbrook, N. J., Plummer, C., Wille, J. D., Favier, V., Crockart, C., Harlan, M., Abram, N., Long, C. A., Nation, M., Christoffersen, P., and King, M.: Weather regimes preclude the observation of a Southern Annular Mode signal in two coastal East Antarctic ice cores. Journal of Geophysical Research: Atmospheres, 131(10), Article e2025JD045013. https://doi.org/10.1029/2025JD045013, 2026.

Uemura, R., Matsui, Y., Yoshimura, K., Motoyama, H., and Yoshida., N.: Evidence of deuterium excess in water vapor as an indicator of ocean surface conditions, J. Geophys. Res., 113, D19114, doi:10.1029/2008JD010209, 2008.

Vance, T. R., Roberts, J. L., Moy, A. D., Curran, M. A. J., Tozer, C. R., Gallant, A. J. E., Abram, N. J., van Ommen, T. D., Young, D. A., Grima, C., Blankenship, D. D., and Siegert, M. J.: Optimal site selection for a high-resolution ice core record in East Antarctica, Climate of the Past, 12(3): 595-610, 2016.

Wille, J. D., Favier, V., Gorodetskaya, I. V., Agosta, C., Kittel, C., Beeman, J. C., Jourdian, N.C., Lenaerts, J.T.M., Codron, F.: Antarctic atmospheric river climatology and precipitation impacts. Journal of Geophysical Research: Atmospheres, 126, e2020JD033788. https://doi.org/10.1029/2020JD033788, 2021.

Winstrup, M., Vallelonga, P., Kjær, H. A., Fudge, T. J., Lee, J. E., Riis, M. H., Edwards, R., Bertler, N. A. N., Blunier, T., Brook, E. J., Buizert, C., Ciobanu, G., Conway, H., Dahl-Jensen, D., Ellis, A., Emanuelsson, B. D., Hindmarsh, R. C. A., Keller, E. D., Kurbatov, A. V., Mayewski, P. A., Neff, P. D., Pyne, R. L., Simonsen, M. F., Svensson, A., Tuohy, A., Waddington, E. D., and Wheatley, S.: A 2700-year annual timescale and accumulation history for an ice core from Roosevelt Island, West Antarctica, Clim. Past, 15, 751–779, https://doi.org/10.5194/cp-15-751-2019, 2019.

Xie, A., Zhu, J., Qin, X., Wang, S., Xu, B., and Wang, Y.: Surface warming from altitudinal and latitudinal amplification over Antarctica since the International Geophysical Year, Sci. Rep., 13, 9536, https://doi.org/10.1038/s41598-023-35521-w, 2023.

Yuan, X.: ENSO-related impacts on Antarctic sea ice: a synthesis of phenomenon and mechanisms. Antarctic Science. 2004;16(4):415-425. doi:10.1017/S0954102004002238, 2004.

Zhang, P. and Duan, A.: Connection between the Tropical Pacific and Indian Ocean and Temperature Anomaly across West Antarctic. npj Clim Atmos Sci 6, 49. https://doi.org/10.1038/s41612-023-00381-8, 2023.

Zhang, L., Ren, X., Cai, W., Li, X., and Wu, L.: Weakened western Indian Ocean dominance on Antarctic sea ice variability in a changing climate. Nat Commun 15, 3261 (2024). https://doi.org/10.1038/s41467-024-47655-0, 2024.

Zhu, J., Xie, A., Qin, X., Wang, Y., Xu, B., and Wang, Y.: An assessment of ERA5 reanalysis for Antarctic near-surface air temperature, Atmosphere, 12, 217, https://doi.org/10.3390/atmos12020217, 2021.